Problem of two fixed centers and a finite dipole: A unified treatment

J. E. Howard
Pacific Dynamics, P. O. Box 1123, Boulder, Colorado 80306-1123

T. D. Wilkerson
Physics Department, Utah State University, Logan, Utah 84322-4415
(Received 12 June 1995)

We investigate the classical dynamics of the problem of two centers and a finite dipole by means of a common Hamiltonian model. Conditions for trapped orbits are determined first by a qualitative analysis of the effective potential, revealing two types of bifurcation in the two-center problem as a control parameter passes through a critical value μ_c. For equal masses there is a pitchfork bifurcation, for unequal masses a tangent bifurcation. Separating the common Hamiltonian in elliptic coordinates shows that the third invariants for the two-center problem and the finite dipole are isomorphic in scaled variables. Explicit trapping conditions are then found in terms of the coefficients of two quartics. A critical-point analysis for the finite dipole shows that a potential well exists for all values of scaled angular momentum below the same critical value μ_c, at which the elliptic point runs off to infinity. In this case the existence of the third invariant does not confine any orbits not already trapped by energy conservation. A similar analysis of the effective potential for the point dipole shows that the only trapped orbits besides those impacting the origin are *unstable* zero-energy trajectories lying on a sphere.

PACS number(s): 33.15.Ry, 03.20.+i, 95.10.Ce, 03.65.Sq

I. INTRODUCTION

Among the oldest and most important problems in dynamics must surely be counted the problem of two fixed centers, which finds myriad applications in celestial mechanics [1–8] as well as in atomic physics [9–13]. First investigated by Euler in 1760, the two-center problem may be viewed as a limiting case of the restricted three-body problem, in which a particle of negligible mass moves in the gravitational field of two massive bodies. As Euler showed, this system enjoys a privileged position in mechanics, inasmuch as it is completely integrable in elliptic coordinates. The solutions were discussed in detail by Legendre and by Jacobi [1], and the possible meridional motions exhaustively classified by Charlier [2] and Deprit [3]. Applications to satellite motion about an oblate planet were discussed by Timoshkova [5] and Aksenov [6]. More recently, Chandrasekhar [7] investigated the scattering of radiation by two black holes with electrostatic repulsion holding the two black holes fixed. Contopoulos [8] subsequently treated the *nonintegrable* relativistic motion of particles and photons near two black holes.

In atomic physics applications the role of the gravitational field is played by the electrostatic field of two charges; the equations of motion are entirely isomorphic. This system was studied by Bohr [9], Pauli [10], Fermi [11], Born [12], and Teller [13], in connection with bound states of the molecular ion H_2^+. Of these, the most definitive is that by Pauli, based on his Ph. D. thesis. Although some of his conclusions regarding possible quantizable states are incorrect in the light of modern wave mechanics, his treatment of the classical motion is impressive. More recently, Strand and Reinhardt [14] have employed uniform Einstein-Brillouin-Keller quantization to determine accurate low-lying states of H_2^+. Here conditions for classical trapped orbits are needed to define quantizable action integrals.

Reversing the sign of one of the charges gives the finite dipole, which has been studied extensively by Turner and Fox [15–17]. These authors show that trapped orbits exist, but do not determine the explicit necessary conditions on physical parameters. If one lets the separation (2a) of the charges to go to zero while simultaneously increasing the charge q such that the dipole strength $p=2aq$ remains constant, one obtains the familiar point dipole [18], which is a member of the class of integrable Stäckel potentials [19,20]. Fox has shown that the only trapped orbits for the point dipole lie on spherical surfaces, so that the only quantal bound states correspond to circular orbits. We confirm this result but find that all such orbits are unstable. One important application of these calculations is the determination of the minimum dipole moment required to trap an electron.

Our primary aim in this paper is to derive explicit algebraic conditions for the existence of stable three-dimensional trapped orbits for each system. Such orbits possess well-defined classical actions, which form the basis for the semiclassical quantization of atomic systems. We first examine the Morse structure of the effective potential, which forms a two-dimensional well which can confine orbits in the presence of closed equipotentials. This approach reveals important features of the motion difficult to discover in the separated equations. Performing a critical-point analysis of the effective potential for the two-center problem, we obtain the critical parameter for the bifurcation of circular orbits, previously found only by approximate methods [11,15]. This is carried out semianalytically for the asymmetric case of unequal masses, for which there is a saddle-node bifurcation, and the equal-mass case, for which the existence of a symmetry line results in a pitchfork bifurcation. These results apply to H_2^+ (equal charges) [14], as well as to asymmetric

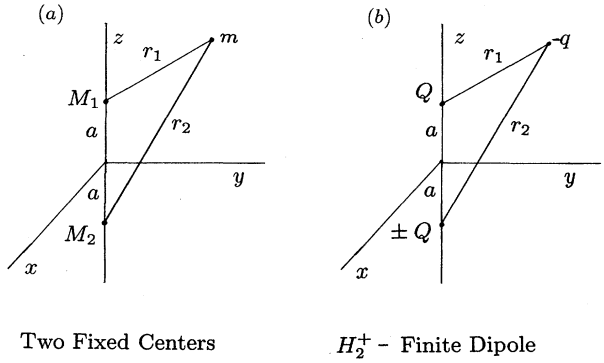

FIG. 1. Test particle moving in the gravitational field of two large masses located at fixed positions $z=\pm a$. The same diagram describes an electron moving in the electric field of two fixed positive charges.

molecular ions such as HeH^{2+}, which has recently been found to possess stable bound states [21]. A similar critical-point analysis for the finite dipole reveals the existence of a potential well, but only for values of the control parameter less than a critical value identical to the bifurcation threshold for the problem of two centers. This critical value is identical to that previously obtained for the point dipole [16], and shows that classical electrons may be trapped by an arbitrarily small dipole moment. These theoretical predictions are well confirmed by numerical orbit calculations.

The reader may question the value of studying the effective potential in cylindrical coordinates when a full solution of the separated equations is available in elliptic coordinates. This approach not only yields increased physical insight, but also provides a method of attacking related *nonintegrable* systems, such as H_2^+ in an axial magnetic field [22]. Another example is the nonintegrable Stark-Zeeman problem [23,24], in which a Rydberg atom is exposed to parallel electric and magnetic fields. Here the effective potential leads directly to a saddle-point criterion for field ionization. Furthermore, many of the bifurcations reported here are quite transparent in cylindrical coordinates and quite difficult to discover in the separated equations.

Even when the equipotential for a given energy is open, the existence of a third invariant can confine orbits. Carrying out the usual separation in elliptic coordinates, we find that the resulting equations for the two-center and finite dipole problems are isomorphic. Consequently the trapping conditions are very similar in scaled variables. As in the closely related Stark problem [12,24], a basic question of some importance is, for what physical parameters do bound states exist? For the systems under consideration here, the answer is given by the reality of the zeros of two quartic polynomials formed from the third invariant, whose coefficients are functions of these parameters. This calculation is performed for the case of equal masses in the problem of two centers as well as the finite and point dipoles. The resulting trapping region for three-dimensional orbits is a complex, simply connected volume in the space of the three invariants. The case of unequal masses is more complicated and will be treated separately [25].

II. HAMILTONIAN MODEL

Consider two large equal masses M lying on the z axis at distances $\pm a$ from the origin, as depicted in Fig. 1(a). The case of unequal masses is also of interest and will be treated in Sec. III. The Hamiltonian for a test particle of mass $m \ll M$ moving in the mutual gravitational attraction of the two large masses is, in cylindrical coordinates (ρ,ϕ,z),

$$H=\frac{1}{2m}(p_\rho^2+p_z^2)+\frac{p_\phi^2}{2m\rho^2}-\frac{GMm}{r_2}-\frac{GMm}{r_1}, \quad (2.1)$$

where G is the universal gravitational constant and

$$r_1^2=\rho^2+(z-a)^2, \quad r_2^2=\rho^2+(z+a)^2, \quad (2.2)$$

and $p_\rho=m\dot{\rho}$, $p_z=m\dot{z}$, and $p_\phi=m\rho^2\dot{\phi}$. Similarly, for a test charge $-q$ moving in the electrostatic field of two massive particles of charge $\pm Q$ [Fig. 1(b)]:

$$H=\frac{1}{2m}(p_\rho^2+p_z^2)+\frac{p_\phi^2}{2m\rho^2}-\frac{\sigma qQ}{r_2}-\frac{qQ}{r_1}, \quad (2.3)$$

where $\sigma=\pm 1$. Note that no restriction is made concerning the magnitude of q/Q. After straightforward scalings, both systems may be described by the common Hamiltonian

$$H=\frac{1}{2}(p_\rho^2+p_z^2)+\frac{\mu}{2\rho^2}-\frac{\sigma}{r_2}-\frac{1}{r_1}, \quad (2.4)$$

where $\mu=p_\phi^2/a^2$ and $a=1$ in (2.2). The *point dipole* is obtained by letting $Q\to\infty$, $a\to 0$ in such a way that the dipole moment $p=2aQ$ remains constant, and will be discussed in Sec. V.

The possible motions in each case are limited by the structure of the effective potential

$$U(\rho,z)=\frac{\mu}{2\rho^2}-\frac{\sigma}{r_2}-\frac{1}{r_1}, \quad (2.5)$$

which depends (for fixed σ) on the single control parameter μ. That is, in the reduced system the particle moves in the two-dimensional potential well $U(\rho,z)$. For a typical nonintegrable system, that is the whole story; energy conservation implies that an orbit of energy $E<E_0$ is confined if and only if the level sets (zero velocity curves) of $U=E_0$ are closed. For integrable systems the addition of a third global invariant further constrains the motion so that confinement is possible even in an open potential well. The form of the various zero-velocity curves so generated will be discussed in detail in Secs. III–V. Before doing so let us set the stage by demonstrating the separability of the Hamiltonian (2.4), by a method somewhat more direct than traditional treatments.

Introducing confocal elliptic coordinates (ξ,η), such that

$$r_1=\xi+\eta, \quad r_2=\xi-\eta, \quad (2.6)$$

it follows that

$$\rho^2=(\xi^2-1)(1-\eta^2), \quad z=-\xi\eta, \tag{2.7}$$

with inverse

$$\xi=\tfrac{1}{2}\left[\sqrt{\rho^2+(z-1)^2}+\sqrt{\rho^2+(z+1)^2}\right],$$
$$\eta=\tfrac{1}{2}\left[\sqrt{\rho^2+(z-1)^2}-\sqrt{\rho^2+(z+1)^2}\right]. \tag{2.8}$$

Note that $\xi\geqslant 1$, $|\eta|\leqslant 1$, so that $\xi^2-1\geqslant 0$, $1-\eta^2\geqslant 0$. The momenta canonically conjugate to (ξ,η) are efficiently found from the generating function

$$S(\rho,z,p_\xi,p_\eta)=\xi(\rho,z)p_\xi+\eta(\rho,z)p_\eta, \tag{2.9}$$

from which

$$p_\rho=\frac{\partial S}{\partial\rho}=\frac{\sqrt{(\xi^2-1)(1-\eta^2)}}{\xi^2-\eta^2}(\xi p_\xi-\eta p_\eta),$$

$$p_z=\frac{\partial S}{\partial z}=-\frac{1}{\xi^2-\eta^2}[\eta(\xi^2-1)p_\xi+\xi(1-\eta^2)p_\eta]. \tag{2.10}$$

Hence the kinetic terms are

$$p_\rho^2+p_z^2=\frac{1}{\xi^2-\eta^2}[(\xi^2-1)p_\xi^2+(1-\eta^2)p_\eta^2]. \tag{2.11}$$

The potential energy is easily evaluated:

$$V=-\frac{\sigma}{r_2}-\frac{1}{r_1}=-\frac{\sigma}{\xi-\eta}-\frac{1}{\xi+\eta}=\frac{-(1+\sigma)\xi+(1-\sigma)\eta}{\xi^2-\eta^2}, \tag{2.12}$$

and therefore

$$(\xi^2-\eta^2)H=\tfrac{1}{2}[(\xi^2-1)p_\xi^2+(1-\eta^2)p_\eta^2]+\tfrac{1}{2}\mu\left[\frac{1}{\xi^2-1}+\frac{1}{1-\eta^2}\right]-(1+\sigma)\xi+(1-\sigma)\eta, \tag{2.13}$$

which is manifestly separable. The separation constant is a function of the dynamical variables and constitutes a third invariant independent of the total energy H and scaled angular momentum μ. Note that this Hamiltonian is invariant to the transformation $\sigma\rightarrow-\sigma$, $\xi\leftrightarrow\eta$. It follows that the problem of two centers and the finite dipole are described by the same scaled equations. In the following two sections we shall exploit this symmetry in determining trapping conditions for each case.

III. TWO FIXED CENTERS

The problem of two fixed centers has a long and distinguished history, attracting the attention of many celebrated mathematicians, despite the lack of the "services of an Archangel" to hold the two massive bodies at a fixed distance [7]. Thus its primary practical interest in celestial mechanics is as a limiting case of the three-body problem, affording some insight into its byzantine complexities.

We begin by carrying out a critical-point analysis of the effective potential, which constitutes a two-dimensional well for the reduced motion. In this picture the critical points represent circular orbits, which are stable or unstable depending on the type of the associated critical point. This is first carried out for the symmetric case of equal masses, which possesses equatorial equilibria which bifurcate via a pitchfork bifurcation into nonequatorial equilibria as the scaled angular momentum μ decreases through a critical value. The asymmetric case (unequal masses) is quite different and will be treated separately [25]. Here there are no equatorial equilibria, and a single *nonequatorial* elliptic critical point exists for sufficiently large μ. As μ decreases, a second elliptic point and a hyperbolic point are born via a tangent bifurcation. Bifurcation thresholds are given explicitly for equal masses and as the solution of an implicit equation for unequal masses.

After working out the stability conditions and bifurcation thresholds, we examine the role of the third invariant in confining particles and its relationship to the potential well $U(\rho,z)$. This leads to a pair of quartic polynomials which form the zero-velocity curves for the third invariant. Analyzing these polynomials gives a pictorial classification of trapped orbits in terms of a set of inequalities among the

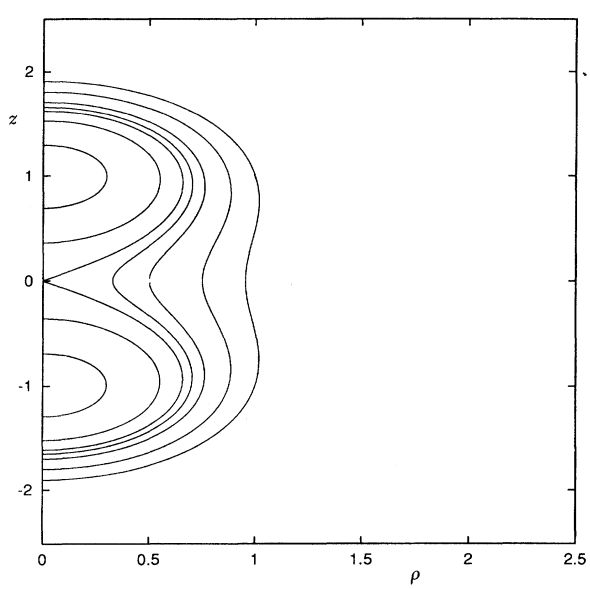

FIG. 2. Level sets of the potential energy $V(\rho,z)$ for the two-fixed-center problem with equal masses.

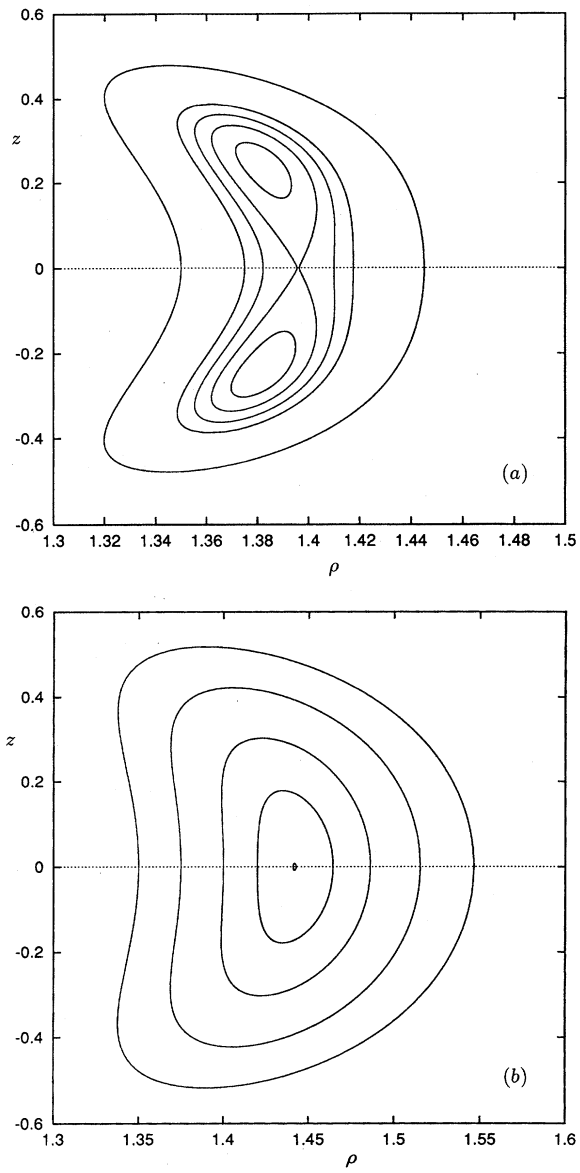

FIG. 3. Level sets of the effective potential $U(\rho,z)$ for the symmetric two-fixed-center problem for control parameters (a) $\mu=1.5$ and (b) 1.6. A double well is formed when μ decreases below $\mu_c=1.5396$.

polynomial coefficients, and thereby the physical parameters E, μ, and α.

A. Critical-point analysis: equal masses

Figure 2 depicts level sets of the potential energy

$$V(\rho,z)=-\frac{1}{r_1}-\frac{1}{r_2}, \tag{3.1}$$

which is useful for analyzing meridional orbits ($\mu=0$). For three-dimensional orbits it is necessary to examine the effective potential

$$U(\rho,z)=\frac{\mu}{2\rho^2}-\frac{1}{r_2}-\frac{1}{r_1}. \tag{3.2}$$

Figure 3 depicts level sets of U for $\mu=1.5$ and 1.6, showing clearly the formation of a double well as μ is reduced to about $\mu=1.54$. The elliptic critical point at the center of each well represents a stable circular orbit, while an unstable circular orbit exists at the saddle point in Fig. 3(a). For $\mu=0$ there is a double well centered at each pole at $z=\pm a$, while the origin is an unstable equilibrium point. A similar bifurcation occurs in the relative motion of two ions in a Paul trap [26,27]. Although Fermi [11] gave an equivalent condition for the existence of nonequatorial circular orbits, he did not supply a derivation or mention the existence of a double well. Turner derived Fermi's condition, but only approximately, by means of a Taylor-series expansion.

Pauli classified three-dimensional orbits as "symmetric," "antisymmetric," and "equatorial." In our nomenclature symmetric orbits are those trapped in a single well, while asymmetric orbits are those trapped in one half of a double well. A third class are all the untrapped orbits ($E>0$). In addition we may distinguish a subclass of orbits trapped in both halves of a double well.

We now derive an explicit condition for the bifurcation seen in Fig. 3. The critical points of U are given by the simultaneous solutions of

$$U_\rho=-\frac{\mu}{\rho^3}+\rho\left[\frac{1}{r_1^3}+\frac{1}{r_2^3}\right]=0,$$
$$U_z=\frac{z-1}{r_1^3}+\frac{z+1}{r_2^3}=0. \tag{3.3}$$

For $\mu=0$ there is a single static equilibrium at the origin, which is easily seen to be unstable (Fig. 2). For $\mu>0$ there are two types of relative equilibria (circular orbits) [28].

Equatorial orbits: When $z_0=0$, $U_z=0$, so that $r_1=r_2=\sqrt{\rho^2+1}$. The equilibrium radius is then given by

$$2\rho^4=\mu(\rho^2+1)^{3/2}, \tag{3.4}$$

which possesses a single positive solution $\rho_0(\mu)$ for all positive μ. This solution may be found as the positive zero of a quartic in $x=\rho^2$.

The type of each critical point is determined by the sign of the Hessian determinant

$$\Delta=\det\begin{pmatrix} U_{\rho\rho} & U_{\rho z} \\ U_{\rho z} & U_{zz}\end{pmatrix}. \tag{3.5}$$

For $\Delta_0<0$, U has a saddle at (ρ_0,z_0); for $\Delta_0>0$ there is a local minimum if $U_{\rho\rho}>0$ and a local maximum if $U_{\rho\rho}<0$. A critical point changes type when Δ_0 passes through zero. Explicitly,

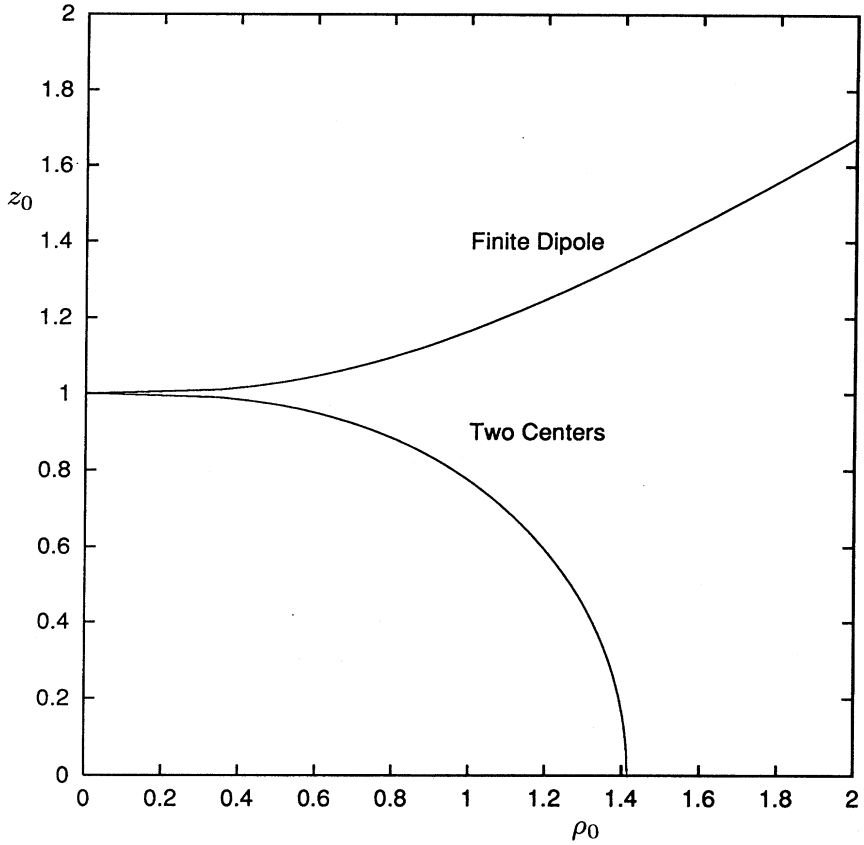

FIG. 4. Locus of relative equilibria (circular orbits) for the symmetric two-center problem and the finite dipole. For two centers (lower curve) there exists a single equatorial equilibrium orbit for all $\mu > \mu_c$ at $\rho_0(\mu)$ given by (3.4). When μ decreases below μ_c this orbit undergoes a pitchfork bifurcation, giving birth to two symmetric nonequatorial circular orbits at (ρ_0, z_0) given by (3.10), and an unstable circular orbit at $\rho_0(\mu)$ given by (3.4). As $\mu \to 0$, $\rho_0 \to 0$ and $z_0 \to 1$. For the finite dipole (upper curve) a single relative equilibria exists for all μ.

$$U_{\rho\rho} = \frac{r_1^2 - 3\rho^2}{r_1^5} + \frac{r_2^2 - 3\rho^2}{r_2^5} + \frac{3\mu}{\rho^4},$$

$$U_{zz} = \frac{r_1^2 - 3(z-1)^2}{r_1^5} + \frac{r_2^2 - 3(z+1)^2}{r_2^5}, \tag{3.6}$$

$$U_{\rho z} = -3\rho\left[\frac{z-1}{r_1^5} + \frac{z+1}{r_2^5}\right].$$

When $z_0 = 0$, $U_{\rho z} = 0$, and (3.6) reduces to $(r = r_1 = r_2)$

$$U_{\rho\rho} = \frac{2}{r^5}(r^2 - 3\rho^2) + \frac{3\mu}{\rho^4},$$

$$U_{zz} = \frac{2}{r^5}(r^2 - 3). \tag{3.7}$$

Note that since V is harmonic, we have, at equilibrium,

$$U_{\rho\rho} + \frac{U_\rho}{\rho} + U_{zz} = \frac{2\mu}{\rho^4} = 2\omega^2, \tag{3.8}$$

where ω is the orbital frequency.

For stability we require $U_{\rho\rho}$, $\Delta = U_{\rho\rho}U_{zz} \geqslant 0$. Thus stability comes down to requiring that $U_{zz} \geqslant 0 \Rightarrow r_0 \geqslant \sqrt{3} \Rightarrow \rho_0 \geqslant \sqrt{2}$. Solving (3.4) for μ we find that $\Delta \geqslant 0$ for $\mu \geqslant \mu_c$, where

$$\mu_c = \tfrac{8}{9}\sqrt{3} = 1.5396\ldots, \tag{3.9}$$

and $E_c = -\frac{4}{9}\sqrt{3} = -0.7698$. That is, when $\mu > \mu_c$ $\exists$ a single elliptic point at $\rho_0(\mu)$ given by (3.3); when μ decreases through μ_c this point becomes hyperbolic (unstable), giving birth to a symmetric pair of nonequatorial elliptic fixed points. The location $\rho_0(\mu)$, $z_0(\mu)$ of the nonequatorial fixed points may be found explicitly by first solving Eq. (3.3b) for ρ^2:

$$\rho^2 = \frac{(1+z)^2(1-z)^{2/3} - (1-z)^2(1+z)^{2/3}}{(1+z)^{2/3} - (1-z)^{2/3}}. \tag{3.10}$$

The corresponding value of μ is then given by Eq. (3.3b). Figure 4 shows the locus of elliptic fixed points (stable circular orbits) in the ρ-z plane as given by (3.10), along with the corresponding locus for the finite dipole. Note that $z \to 1$ as $\rho \to 0$, so that as $\mu \to 0$ the equilibrium tends toward the source at (0,1). Explicitly, near this point $\rho_0 \approx \mu$ and $z_0 \approx 1 - \frac{1}{4}\mu^3$. For large z, $\rho_0 \approx \sqrt{2}z_0$. The stability of these circular orbits has been verified by numerical evaluation of the Hessian determinant.

Normal modes

It is also of interest to calculate normal mode frequencies for the stable equilibria in Fig. 4. For example, in H_2^+ these libration frequencies may be excited by microwave radiation and correspond to quantum-mechanical states with small elliptic quantum numbers. In general, for positive definite ki-

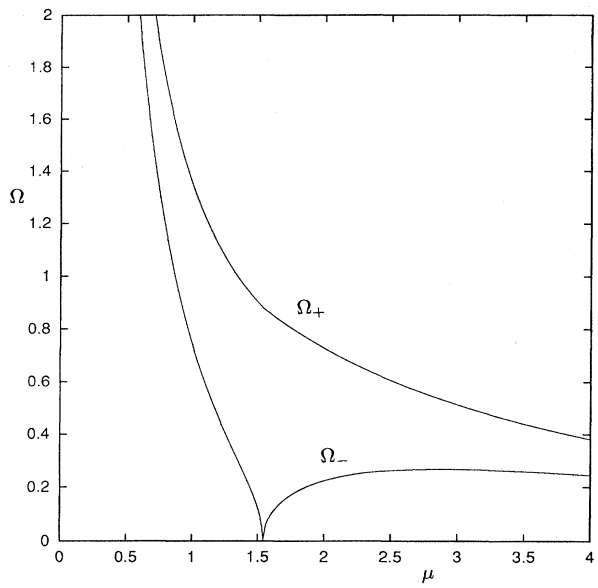

FIG. 5. Normal-mode frequencies for the symmetric two-center problem as a function of μ. The slow mode Ω_- drops rapidly to zero when $\mu \to \mu_c$.

netic energy the normal mode frequencies $\Omega_\pm$ are given by the eigenvalues $\Lambda = \Omega^2$ of the Hessian matrix $\mathscr{H} = D^2 U$, i.e.,

$$\det(\mathscr{H} - \Lambda \mathbf{I}) = 0 \tag{3.11}$$

or

$$\Lambda^2 - \mathrm{Tr}\mathscr{H}\Lambda + \det\mathscr{H} = 0 \tag{3.12}$$

so that

$$2\Omega_\pm^2 = \mathrm{Tr}\mathscr{H} \pm \sqrt{(\mathrm{Tr}\mathscr{H})^2 - 4\det\mathscr{H}}, \tag{3.13}$$

where

$$\mathrm{Tr}\mathscr{H} = U_{\rho\rho} + U_{zz} = -\frac{2}{r^5} + \frac{3\mu}{\rho^4}. \tag{3.14}$$

Unfortunately, $\Delta = \det\mathscr{H}$ does not simplify appreciably. For equatorial circles the normal modes lie along the ρ and z axes, but tilt somewhat for the nonequatorial equilibria. The variation of $\Omega_\pm$ with μ is depicted in Fig. 5. Note that Ω_- vanishes for $\mu = \mu_c$; for $\mu > \mu_c$ this mode is purely vertical. The second mode, Ω_+, decreases monotonically with in-

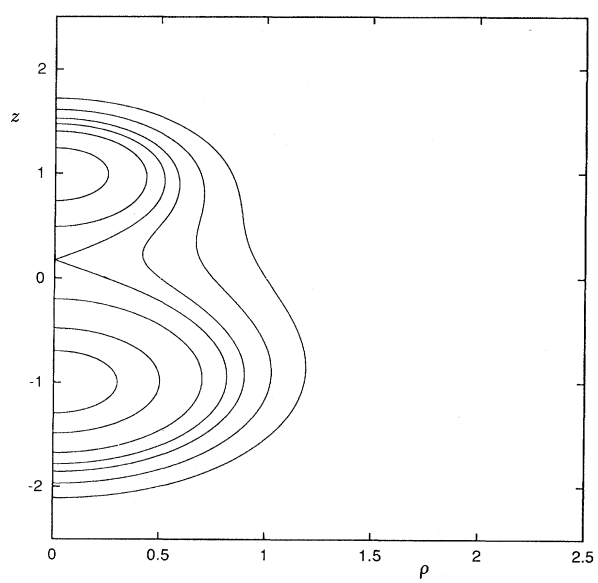

FIG. 6. Level sets of the potential $V(\rho,z)$ for the asymmetric two-center problem with mass ratio $\gamma = M_2/M_1$.

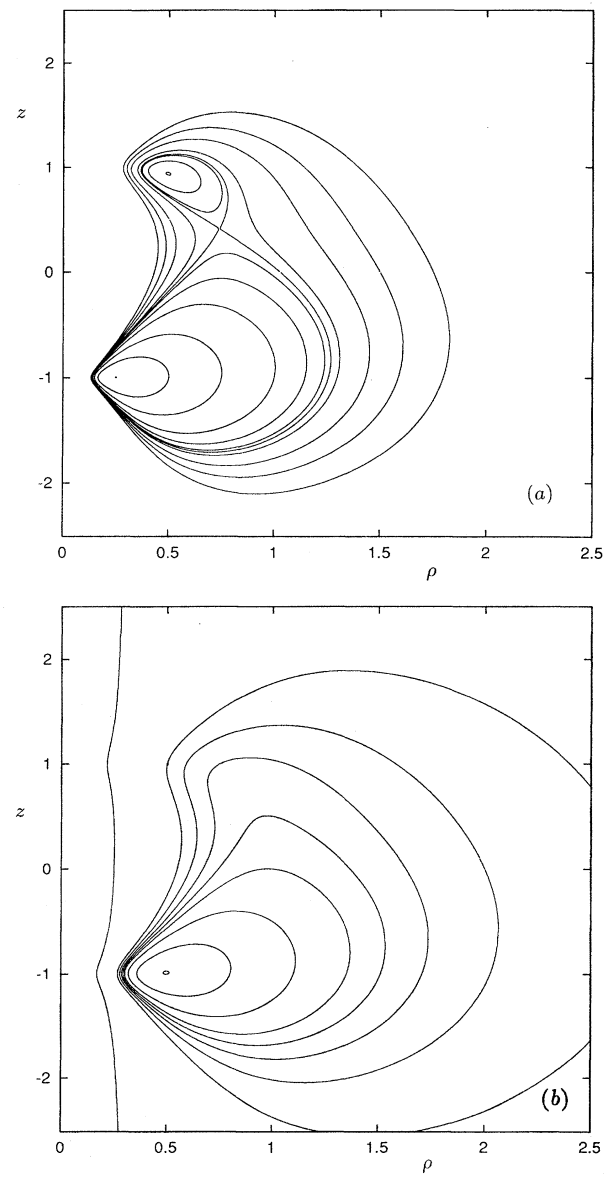

FIG. 7. Level sets of the effective potential $U(\rho,z)$ for two fixed centers with mass ratio $\gamma = 2$ and (a) $\mu = 0.5$ and (b) $\mu = 1$. A double well is formed via a tangent bifurcation when μ is decreased below $\mu_c = 0.742$.

creasing μ, and is purely radial for $\mu > \mu_c$. The two modes are never degenerate, except perhaps asymptotically for large or small μ. For moderate μ we may therefore speak of a slow mode and a fast mode. It would be interesting to see whether these modes could be excited in laboratory experiments.

B. Critical-point analysis: unequal masses

The potential energy (3.1) is readily generalized to encompass unequal masses by means of the dimensionless mass ratio

$$\gamma = M_2/M_1, \tag{3.15}$$

so that

$$V(\rho,z) = -\frac{1}{r_1} - \frac{\gamma}{r_2}. \tag{3.1a}$$

Figure 6 shows the form of the potential contours for $\gamma=2$. It is then straightforward to modify the algebra of Sec. III A. Thus the equilibrium conditions on the effective potential become

$$U_\rho = -\frac{\mu}{\rho^3} + \rho\left[\frac{1}{r_1^3} + \frac{\gamma}{r_2^3}\right] = 0,$$

$$U_z = \frac{z-1}{r_1^3} + \gamma\frac{z+1}{r_2^3} = 0. \tag{3.3a}$$

For $\gamma \neq 1$ there are clearly no equatorial equilibria. In order to gain a preliminary view of the structure of $U(\rho,z)$, Fig. 7 plots level sets of U for $\gamma=2$ and $\mu=0.5$ and 1. As in the case of equal masses there is a single elliptic fixed point for large μ. Now, however, a double well is formed through a tangent bifurcation at a critical control parameter $\mu_c = \mu_c(\gamma)$.

The general features of these potential curves can be understood from the locus of equilibria Γ, which follows from the second of Eqs. (3.3a):

$$\rho^2 = \frac{(1+z)^2(1-z)^{2/3} - \gamma^{2/3}(1-z)^2(1+z)^{2/3}}{\gamma^{2/3}(1+z)^{2/3} - (1-z)^{2/3}}. \tag{3.10a}$$

Figure 8 plots Γ for $\gamma=2$, revealing the existence of two branches to the equilibrium locus. The lower branch Γ^- $(z_0<0)$ emanates from the point $z_0=-1$, exists for all $\mu>0$, and is asymptotic to the line

$$\lim_{\rho_0\to\infty} z_0 = -\frac{\gamma-1}{\gamma+1}. \tag{3.16}$$

The upper branch Γ^+ $(z_0>0)$, on the other hand, exists only for μ less than a critical value depending on γ. The upper part of this loop traces the stable critical point, terminating at $z_0(0)=+1$, while the lower half traces the unstable point, terminating at

$$\lim_{\rho_0\to 0} z_0(\rho_0) = \frac{\sqrt{\gamma}-1}{\sqrt{\gamma}+1}, \tag{3.17}$$

which is just the location of the x point in Fig. 6. It should be noted that while there is a point on Γ where the slope is vertical $(U_{zz}=0)$, this point does *not* coincide with the bifurcation point, as indicated in Fig. 8. Since $\Delta<0$ when $U_{zz}=0$ it follows that the former point lies on the unstable part of Γ^+. A similar locus occurs for the Stark problem [24], in which elliptic and hyperbolic fixed points annihilate in a tangent bifurcation.

The critical value of μ may be found by the following procedure: first eliminate μ by substituting $\mu(\rho,z)$ from the first of Eqs. (3.3a) into $U_{\rho\rho}$. Then substitute ρ^2 from (3.10a) into $\Delta(\rho,z) = U_{\rho\rho}U_{zz} - U_{\rho z}^2$, which may be simplified to

$$\Delta(\rho,z) = \frac{1}{r_1^8}[r_1^2 - 9(z-1)^2] + \frac{\gamma^2}{r_2^8}[r_2^2 - 9(z+1)^2] + \frac{2\gamma}{r_1^5 r_2^5}[r_1^2 r_2^2 - 9(z^2-1)^2 + 9\rho^2(z^2-1)] = 0. \tag{3.18}$$

Solving this complicated equation numerically for z_c, ρ_c and μ_c follow straightforwardly by back substitution. Although we have not been able to effect a complete analytic solution to this problem, we have proven several properties of the locus of equilibria. It is shown in the Appendix that for arbitrary smooth axisymmetric potentials μ reaches an extremum at the bifurcation point, which for the two-center problem is a local maximum.

C. Particle trapping

We now return to the general question of particle trapping, which we investigate for the case of equal masses. The case of unequal masses requires using Sturm's theorem [29] and will be reported elsewhere [25]. We have seen that for $\mu<\mu_c$ the effective potential has a single well; all particles with $E<0$ are confined, while those with $E\geqslant 0$ escape to infinity. We call this global trapping. For $\mu>\mu_c$ there is a double well separated by a saddle point on the ρ axis. In this case a particle with $E<E_s$ is forever confined in one of the two wells, a situation we shall refer to as local trapping. The analogous effect in the Stark problem is known as saddle-point confinement [24]. Just as in the Stark problem, the existence of a third invariant can confine particles (here only locally) even when $E>E_s$.

The saddle-point energy is

$$E_s = -\frac{2}{\sqrt{\rho_0^2+1}} + \frac{\mu}{2\rho_0^2} = -\frac{\mu}{2\rho_0^4}(2\rho_0^2+1), \tag{3.19}$$

where ρ_0 is the saddle-point radius, given numerically by (3.4). For $\mu \ll 1$, (3.4) has the expansion

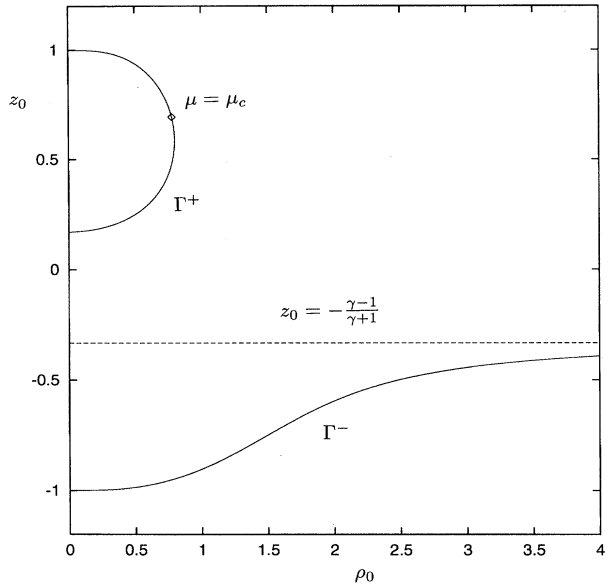

FIG. 8. Loci of relative equilibria for the asymmetric two-center problem for $\gamma=2$. A stable critical point moves along the lower branch Γ^- and is asymptotic to the horizontal line $z_0=-(\gamma-1)/(\gamma+1)$ as $\rho_0\to\infty$. The upper branch exists for $0<\mu<\mu_c$ and consists of two subbranches: the lower twig traces the x point and the upper half-loop the upper O point.

$$\rho_0\approx(\mu/2)^{1/4}\left[1+\frac{3}{2}\left(\frac{\mu}{2}\right)^{1/2}\right], \tag{3.20}$$

so that

$$E_s\approx-1-2\sqrt{\mu/2}. \tag{3.21}$$

Figure 9 illustrates typical trapped and untrapped orbits in the double well for $\mu=1.5$, for which $\rho_0=1.396$ and $E_s=-0.779\,83$. In Fig. 9(a), with $E=-0.779\,75>E_s$, the particle is confined by the third invariant to the upper half of the potential well labeled $U=E$. In Fig. 9(b), with the same energy, but a different value of the third invariant, the orbit is able to explore the entire well. These orbits demonstrate the ability of the third invariant to overrule the topology of the effective potential, constraining the orbit to one half of a single well, even when the particle possesses sufficient energy to explore the entire well. In this section we determine the precise connections between the critical-point analysis of Sec. III B and the effects of the third invariant α, which imposes its own double-well structure.

Just as energy conservation limits the region of physical space available to a particle of energy E, so does the constancy of the third invariant yield its own set of zero-velocity curves. To see this, let us rewrite the Hamiltonian (2.13) in separated form

$$\begin{aligned}\tfrac{1}{2}(\xi^2-1)p_\xi^2+\frac{\mu}{2(\xi^2-1)}-E\xi^2-2\xi&=-\alpha,\\ \tfrac{1}{2}(1-\eta^2)p_\eta^2+\frac{\mu}{2(1-\eta^2)}+E\eta^2&=+\alpha,\end{aligned} \tag{3.22}$$

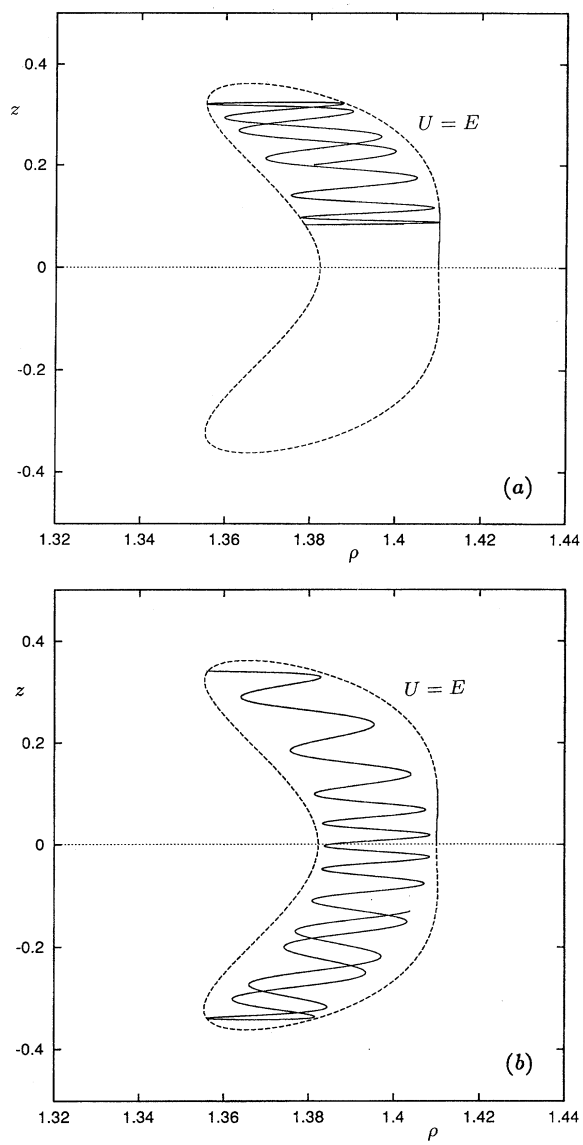

FIG. 9. Trapped and untrapped orbits in the double well of the symmetric two-center problem. Energies are in scaled atomic units.

where the separation constant α is the third invariant. Erickson and Hill [30] have shown that the third invariant is equivalent to the geometric quantity

$$\Omega=\mathbf{L}_1\cdot\mathbf{L}_2+2(\cos\theta_1-\cos\theta_2), \tag{3.22a}$$

where $\mathbf{L}_1$ and $\mathbf{L}_2$ are the angular momenta of the test particle with respect to the two source masses, and θ_1 and θ_2 are the respective central polar angles of $\mathbf{r}_1$ and $\mathbf{r}_2$. An elegant generalization of this result is given by Coulson and Joseph [31], who point out the connection with the Runge-Lenz vector for the Kepler problem. It is readily shown that

$$\Omega=|E|+\alpha, \tag{3.22b}$$

a relation which will prove useful in classifying orbits.

Since the first term in each of equations (3.22) is nonnegative, it follows that

$$\frac{\mu}{2(\xi^2-1)}-E\xi^2-2\xi\leqslant-\alpha,$$
$$\frac{\mu}{2(1-\eta^2)}+E\eta^2\leqslant+\alpha, \tag{3.23}$$

which correspond precisely to $U\leqslant E$. For negative-energy trapped orbits, inequalities (3.23) are equivalent to

$$F(\xi)=\xi^4-A\xi^3-B\xi^2+A\xi-C\leqslant 0,$$
$$G(\eta)=\eta^4-B\eta^2-C\leqslant 0, \tag{3.24}$$

with

$$A=\frac{2}{|E|},\quad B=1-\frac{\alpha}{|E|},\quad C=\frac{1}{|E|}\left(\alpha-\frac{\mu}{2}\right). \tag{3.25}$$

Thus, we have the following.

Proposition I. An orbit with parameters (E,μ,α) is trapped iff (if and only if) *both* (i) $F(\xi)$ is negative between two positive zeros (ξ_1,ξ_2) with $\xi_1\geqslant 0$ and $\xi_2\geqslant 1$, and (ii) $G(\eta)$ is negative between two zeros (η_1,η_2), with $\eta_1\in[-1,1]$ and $\eta_2\geqslant 0$.

This much may be found in equivalent form in the treatments of Charlier [2] and Pauli [10]. Pauli derived algebraic trapping conditions for equal masses by expressing the coefficients A, B, and C as functions of the zeros of F and G. Charlier's analysis allowed unequal masses and arbitrary energy but was limited to meridional orbits. Strand and Reinhardt [14] also carried out an orbital taxonomy for $E<0$ and $\mu=0$. For comparison, their parameter $\tilde{M}^2$ is equivalent to our μ, and their $-\tilde{\gamma}$ to our α. We shall obtain trapping conditions by a somewhat more geometrical approach. In addition, our method yields explicit conditions for transitions between the various classes of trapped orbits. We begin with a qualitative description of Charlier's four classes of trapped meridional orbits.

Meridional orbits

When $\mu=0$, all orbits lie in a plane of constant ϕ. Although such planar orbits have been thoroughly investigated we briefly discuss them in order to set the stage for the more complicated three-dimensional case. We also emphasize the connections between orbital topology and functional properties of F and G. Our results are summarized in Fig. 10, which depicts Charlier's four classes of trapped meridional orbits, along with the corresponding plots of $F(\xi)$ and $G(\eta)$. Following this qualitative description we derive explicit conditions for each of these classes and transitions between them.

The first type is a pendular libration along the z axis, with $\xi=0$. There are two subclasses, one with η running between limits $\eta_{\max}=\pm 1$ and a second with η running from $|\eta_{\min}|<1$ to $\eta_{\max}=\pm 1$. Thus an orbit in either of these classes eventually collides with one of the masses. While the second subclass is stable, an orbit in the first is not, as it must pass through the hyperbolic point at the origin. The second class ("planetary") occupies an annular region between two concentric ellipses $\xi=\xi_1$ and ξ_2, with η assuming all possible values in $[-1,1]$. The motion is conditionally periodic, with a typical orbit ergodically filling the annulus. When $\xi_1=\xi_2$ this region shrinks to a single ellipse with foci at $z=\pm 1$. The third class, dubbed "satellite" orbits by Charlier, occupies one of two regions bounded by a single ellipse $\xi=\xi_2$ and two branches of an hyperbola $\eta=\pm\eta_1$. Again the motion is ergodic save for a denumerable set of periodic orbits. The fourth class ("lemniscates") fills a region bounded by a single ellipse $\xi=\xi_2$.

Let us now derive algebraic conditions on α and E for each of these classes. In general, satisfying the conditions on the zeros of F and G implied by Proposition I requires Sturm's theorem [29]. For equal masses, however, the connections among the polynomial coefficients permit a simpler analysis. A further simplification occurs for $\mu=0$, where both $F(\xi)$ and $G(\eta)$ factor:

$$F(\xi)=(\xi^2-1)(\xi^2-A\xi+C)=(\xi^2-1)\hat{F}(\xi),$$
$$G(\eta)=(\eta^2-1)(\eta^2+C). \tag{3.26}$$

Thus $F(\pm 1)=G(\pm 1)=0$ and $F(0)=G(0)=-\alpha/|E|$, while $\lim_{\xi\to\pm\infty}F(\xi)=\lim_{\eta\to\pm\infty}G(\eta)=+\infty$.

(i) *Pendular orbits.* An orbit lies on the z axis iff $\xi=+1$. This requires that $F(\xi)$ have a minimum or an inflection point there, i.e., $F'(1)=0$ and (a) $F''(1)>0$ or (b) $F''(1)=0$. From (3.24), setting $F'(1)=0$ gives $\alpha+|E|=2$, for which $(|E|/8)F''(1)=1-\alpha$. Thus there is a local minimum for $\alpha<1$ and an inflection point when $\alpha=1$. [The third choice, $\alpha>1$, for which F has a local *maximum* at $\xi=1$, can be shown to be a particular case of class (iv), described below.] Assume, then, that $\alpha\leqslant 1$. If $\alpha>0$ then $G(0)<0$ and $G(\eta)$ has no zeros in (0,1), as sketched in Fig. 10(ia). If $\alpha<0$ then $G(0)>0$ so that $G(\eta)$ has a zero $\eta_1=\sqrt{-\alpha/|E|}$ in (0,1). Thus $G<0$ in $(\eta_1,1)$, as shown in Fig. 10(ib). Hence the two subclasses are (ia) $0<\alpha<1$: single orbit along $[-1,1]$, and (ib) $\alpha<0$: two orbits along $[\pm\eta_1,\pm 1]$. The boundary for transitions between these two subclasses is the point $\alpha=0$. Geometrically, $F'(1)=\Omega-2$ and $G'(1)=2\Omega/|E|$.

(ii) *Planetary orbits.* This class is sandwiched between two ellipses: $\xi=\xi_1$, ξ_2, which implies that $F(\xi)$ (and therefore $\hat{F}$) possesses two zeros >1, as depicted in Fig. 10(ii). This is true iff $A,B>1$ and $\Delta(\hat{F})=A^2-4C>0$, which is equivalent to $\alpha+|E|>2$, $\alpha|E|<1$, and $\alpha>1$. Geometrically, these conditions ensure that $F(0)=G(0)<0$, $F'(1)>0$, and $G'(1)>0$. Figure 11 depicts the region in the α-$|E|$ plane corresponding to planetary orbits. Note that the functional constraints on G are automatic; an orbit confined to the annular region $\xi_1<\xi<\xi_2$ must *necessarily* explore the entire range of η.

(iii) *Satellite orbits.* These orbits occupy two disconnected regions between the ellipse $\xi=\xi_2$ and the two branches of the hyperbola $\eta=\pm\eta_1$, which implies that $F(\xi)$ possesses a single zero >1, as shown in Fig. 10(iii). This holds iff $0<\Omega<2$ and $\alpha<0$, as indicated in Fig. 11.

(iv) *Lemniscate orbits.* These orbits encircle both masses, filling the entire region within an ellipse $\xi=\xi_2$, as shown in Fig. 10(iv). As in case (iii) $F(\xi)$ must have a single zero >1, again implying $0<\Omega<2$. Now, however, α must be *positive* in order that $\eta\in[-1,1]$. The corresponding region in the α-$|E|$ plane is indicated in Fig. 11. The boundary

between lemniscates and satellite orbits is the vertical line segment, $\alpha=0$, $|E|<2$, and the boundary between lemniscates and planetary orbits is the segment $\Omega=0$, $1<\alpha<2$.

Three-dimensional orbits

When $\mu>0$ there are only two topologically distinct classes of orbits to consider, owing to the fact that the centrifugal barrier excludes the possibility that $\xi_1=1$ or $\eta_2=1$. Figure 12 depicts these classes, along with the corresponding plots of $F(\xi)$ and $G(\eta)$. The first type forms a single well, with $\xi_1<\xi<\xi_2$ and $|\eta|<\eta_2$. The second type forms a double well, with $\eta_1<\eta<\eta_2$. How is the transition between these types related to the pitchfork bifurcation of Sec. III A? In order to answer this question, let us derive

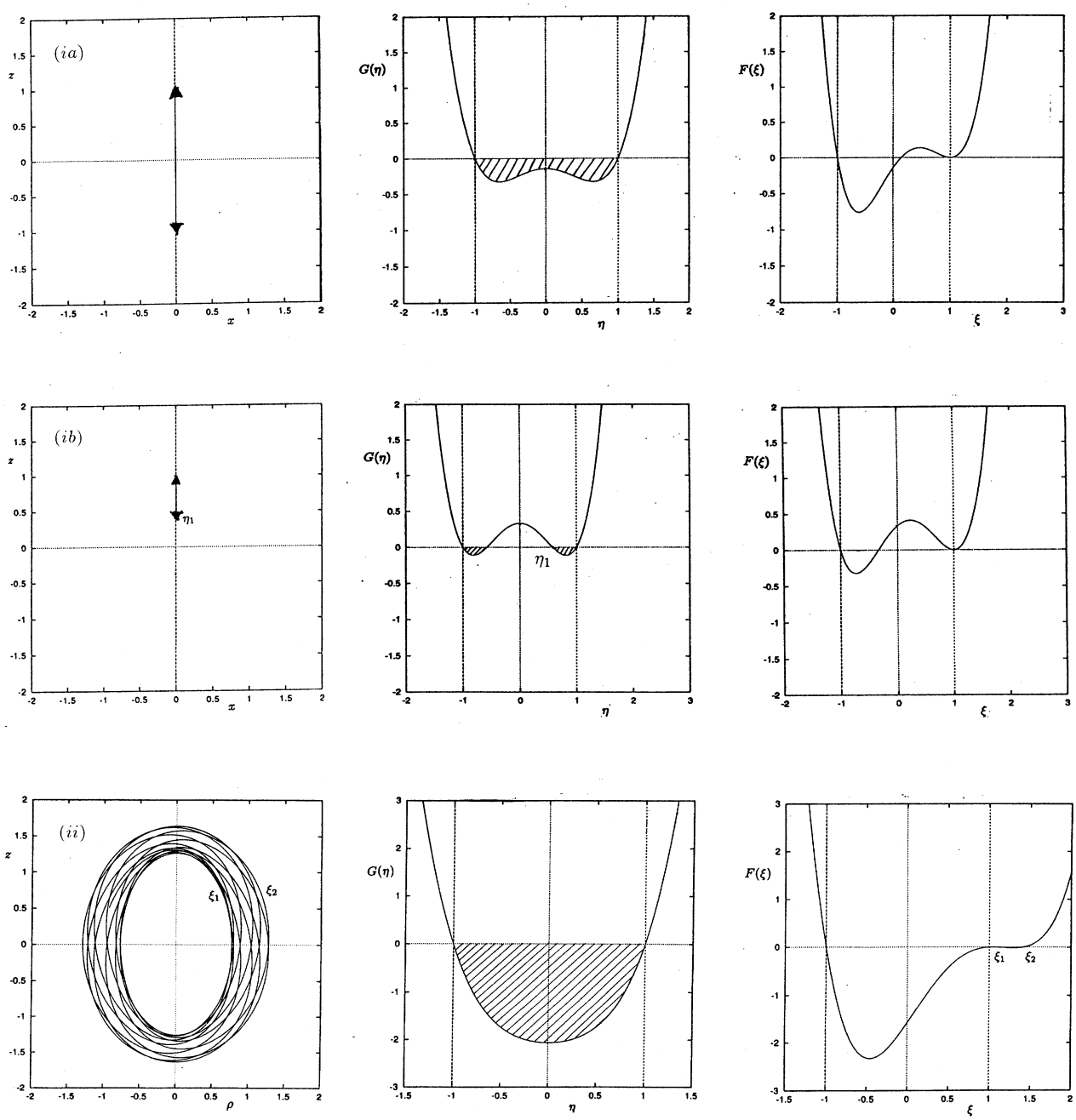

FIG. 10. The four classes of trapped meriodional orbits ($\mu=0$) for the symmetric two-center problem, along with the trapping polynomials $F(\xi)$ and $G(\eta)$ for each class: (i) Pendular orbits, confined to the z axis with (a), $\alpha>0$; and (b) $\alpha<0$. (ii) Planetary orbits, sandwiched between ellipses $\xi=\xi_1$ and ξ_2. (iii) Satellite orbits, confined by the ellipse $\xi=\xi_2$ and one of the two branches of the hyperbola $\eta=\pm\eta_1$. (iv) Lemniscates, which encircle both masses, filling the entire region within the ellipse $\xi=\xi_2$. The satellite and lemniscate orbits are taken from Figs. 8 and 9 in Strand and Reinhardt [14], used by permission.

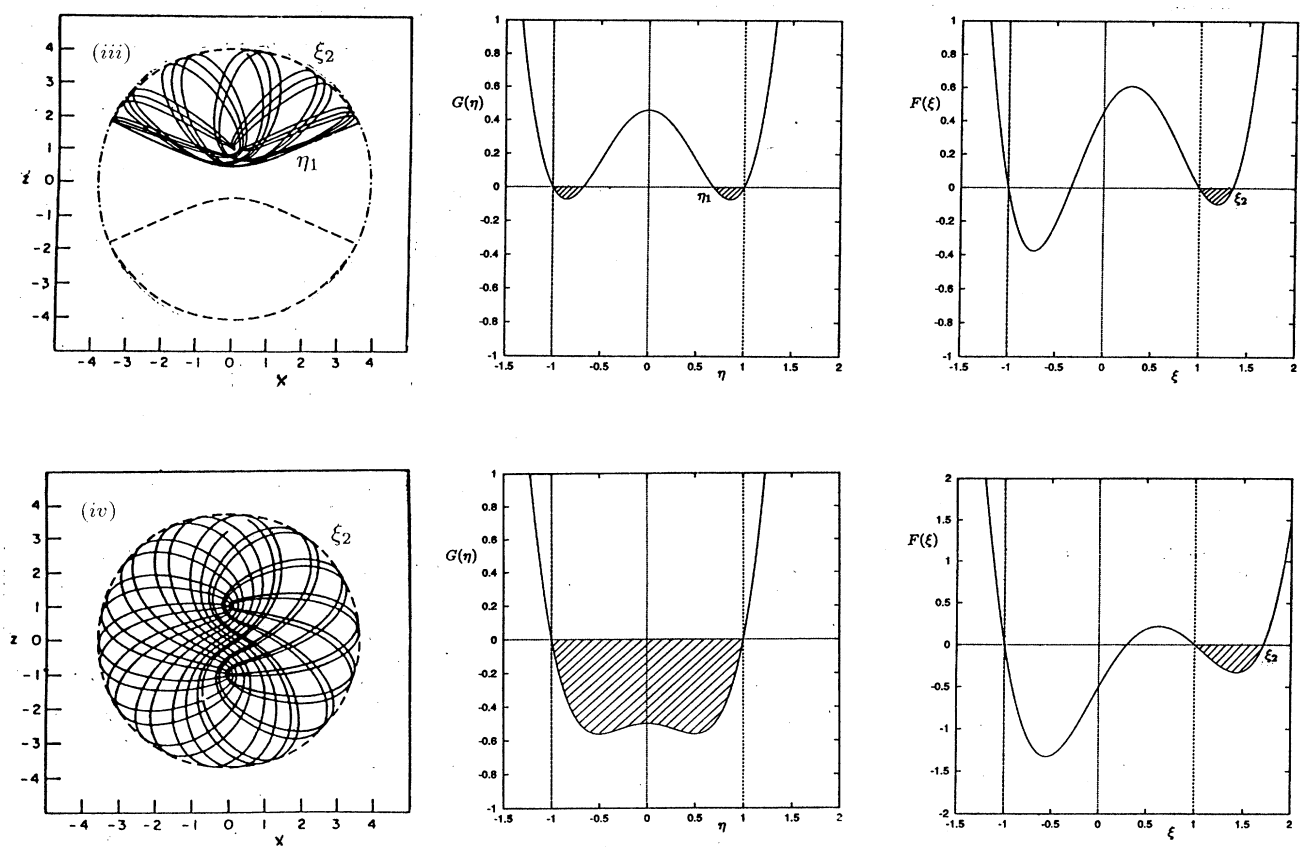

FIG. 10 (*Continued*).

conditions on the coefficients A, B, and C for each class. Our task is complicated by the fact that F and G no longer factor when $\mu>0$, necessitating the calculation of the discriminant Δ of the quartic $F(\xi)$. In all cases $F(0)=G(0)=-(1/|E|)(\alpha-\mu/2)$ and $F(\pm 1)=G(\pm 1)=\mu/2|E|>0$. Also, $F'(\pm 1)=\pm(2/|E|)(\Omega\mp 2)$ and $G'(\pm 1)=\pm 2\Omega/|E|$.

(i) *Single well.* From Fig. 12 we see that the distinguishing feature is the sign of $F(0)=G(0)$, which in this case

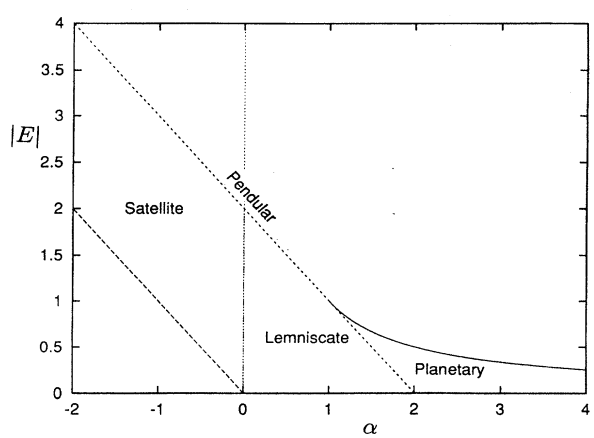

FIG. 11. Trapping region in the α-$|E|$ plane for meridional orbits in the symmetric two-center problem.

must be negative, so that $\alpha>\mu/2$. Since $G(0)<0$ and $G(1)>0$, a zero η_2 between 0 and 1 is guaranteed. Similarly, $F(\xi)$ always has a zero in $(-1,0)$. It follows that $\exists$ real zeros ξ_1, $\xi_2>1$ iff $\Delta(F)>0$.

(ii) *Double well.* Here we need $F(0)=G(0)>0$, which implies that $\alpha<\mu/2$. As a glance at Fig. 12 will show, G does not necessarily possess real zeros η_1, $\eta_2\in(0,1)$. This is the case iff $\Delta(G)>0$ and $0<B<2$, which implies $\Omega^2>2\mu|E|$ and $-|E|<\alpha<|E|$. The last condition is equivalent to $\Omega>0$, so that $G'(1)$ is positive. The constraints on $F(\xi)$ are rather subtle. As a glance at Fig. 12(a) will show, trapping is lost when the positive zeros (ξ_1,ξ_2) merge and become complex, which means $\Delta(F)=0$. However, since $F(0)$ and $F(-1)$ are both positive, it is conceivable that $F(\xi)$ have a negative double zero. Hence, $\Delta(F)=0$ does not necessarily imply loss of trapping. Furthermore, for a general quartic $\Delta(F)$ can vanish when two complex zeros merge. The extraneous configurations may be eliminated by Sturm's theorem [29], which yields necessary and sufficient conditions that a polynomial have N zeros in a specified interval (a,b). Fortunately, owing to the interdependence of the coefficients of F and G, the trapping boundaries can be determined semianalytically, as follows.

The discriminant of F is given by [29]

$$27\Delta(F)=4[3A^2+B^2-12C]^3-[9C(3A^2+8B)+9A^2(B-3)+2B^3]^2. \tag{3.27}$$

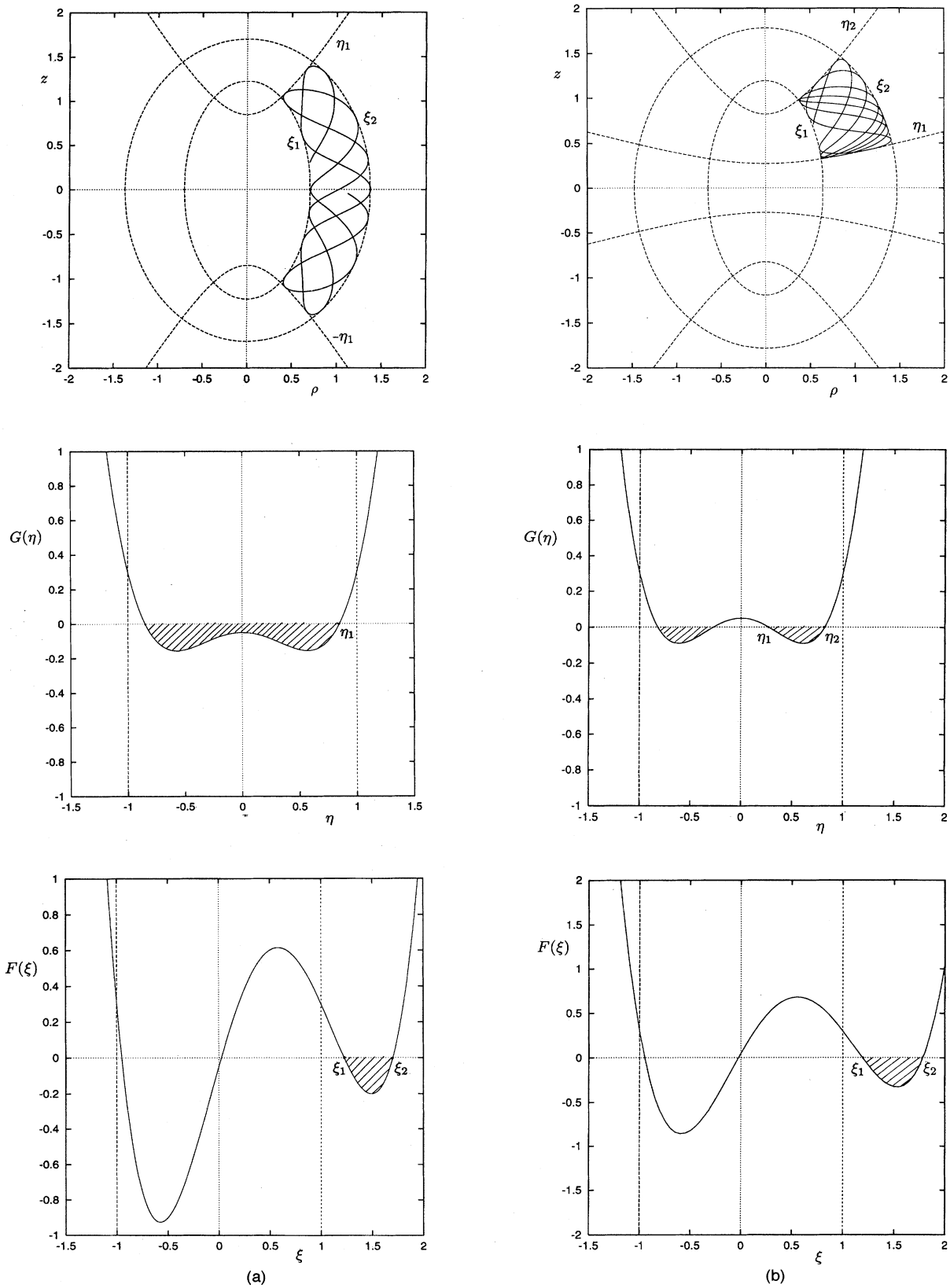

FIG. 12. The two classes of trapped three-dimensional orbits ($\mu>0$) for the symmetric two-center problem, along with the corresponding trapping polynomials F and G for $E=-1$, $\mu=0.6$, and (a) single well ($\alpha=0.35$) and (b) double well ($\alpha=0.25$).

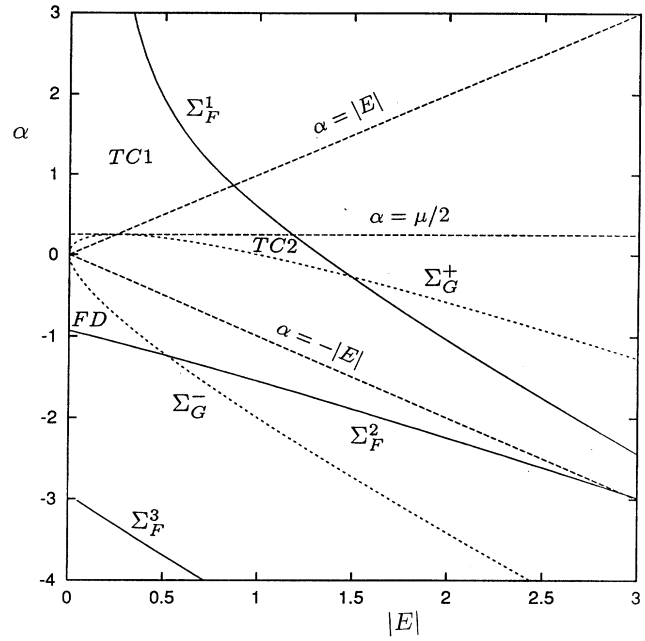

FIG. 13. Trapping regions in the $|E|$-α plane for two centers, with $\mu=0.5$. The discriminant $\Delta(F)$ vanishes along the curves labeled Σ_F^i, $i=1$, 2, and 3, while $\Delta(G)=0$ on $\Sigma_G^{\pm}$. The single-well region ($TC1$) is bounded by Σ_F^1, the line $\alpha=\mu/2$, and the positive α axis. The double-well region ($TC2$) is bounded by Σ_F^1 and Σ_G^+, and the lines $\alpha=\mu/2$ and $|E|=0$; the small region above the origin is eliminated by the condition $\alpha<|E|$. The trapping region for the finite dipole (FD) is bounded by Σ_F^2, Σ_G^-, and the negative α axis.

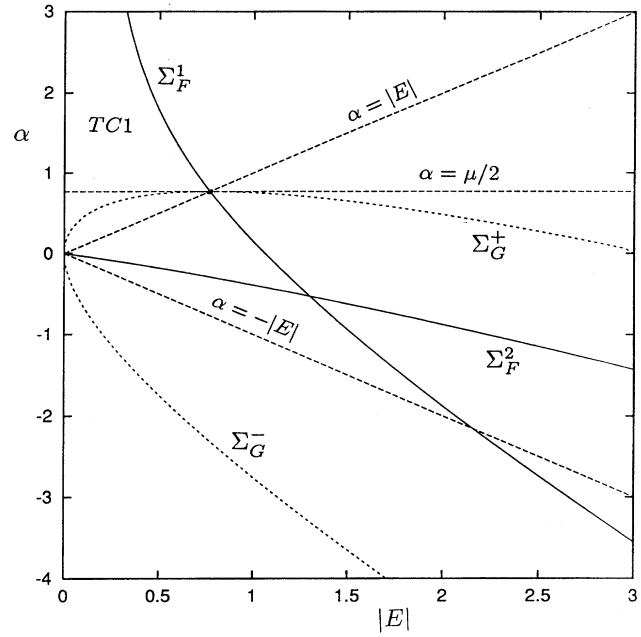

FIG. 14. Trapping regions in the $|E|$-α plane for two centers, with $\mu=\mu_c$. In this transition case the curves (actually surfaces) all intersect at the point $\alpha=|E|=1$. Thus the double-well region $TC2$ shrinks to the point $\alpha=|E|=1$, with $TC1$ bounded as shown. Since Σ_F^2 passes through the origin, the finite dipole region is also cut off.

First note that in order to satisfy $\Delta(F)=0$ the first expression on the right-hand side must be positive. A little numerical exploration reveals that this condition is always satisfied for parameters of interest. The conditions $\Delta(F)=0$, $\Delta(G)=0$ define surfaces Σ_F,Σ_G which partition the space $|E|,\alpha,\mu$ into regions of positive and negative $\Delta(F)$ and $\Delta(G)$. This partition also holds for the finite dipole, to be discussed in Sec. IV. Figure 13 depicts level sets of Σ_F and Σ_G in the $|E|$-α plane for $\mu=0.5$. The surface Σ_G is easily seen to be the parabola

$$\alpha=-|E|\pm\sqrt{2\mu|E|}, \tag{3.28}$$

which tends to the line $\alpha=-|E|$ as $\mu\to 0$. It is convenient to label the upper and lower halves $\Sigma_G^{\pm}$, respectively. We leave it to the reader to verify the following.

Lemma. The plane $\alpha=\mu/2$ is tangent to the surface Σ_G along the line $\alpha=|E|=\mu/2$.

Since $\Delta(G)<0$ inside Σ_G, the trapping region must lie outside this region. The surface Σ_F has three sheets, labeled $\Sigma_F^{1,2,3}$. For the two-center problem, the condition $\alpha<|E|$ restricts attention to Σ_F^1, where $\xi_1=\xi_2$. The other two sheets correspond to negative double zeros. The sheets Σ_F^1 and Σ_F^2 intersect at a point where $F(\xi)$ has *two* double zeros. The trapping region is thus the wedge-shaped region bounded by Σ_G^+ and Σ_F^1 and the positive α axis. Thus trapped orbits exist for arbitrarily large α and $E>E_{\min}$, where Σ_F^1 and Σ_G^+ inter-

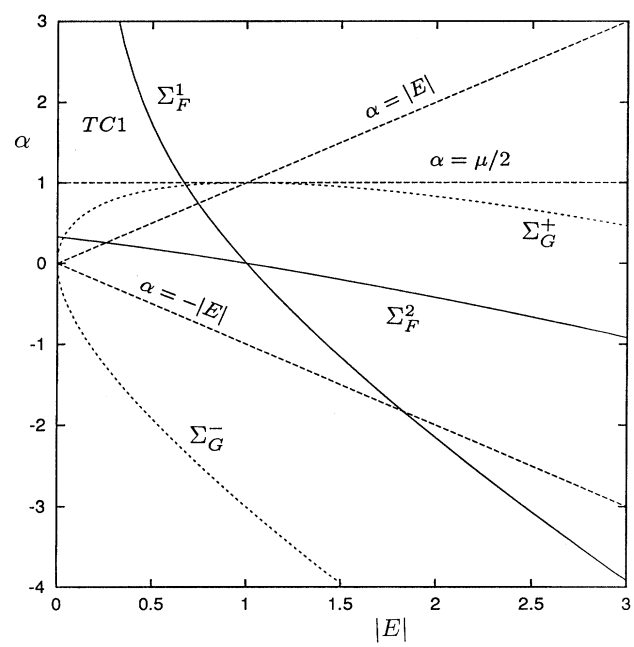

FIG. 15. Trapping region in the $|E|$-α plane for two centers, with $\mu=2.0$. Since $\mu>\mu_c$ there are no double-well orbits. Single-well orbits, on the other hand, exist for arbitrarily large α and μ. Since Σ_F^2 crosses the α axis at a positive value of α, there are no trapped finite-dipole orbits (see Fig. 21).

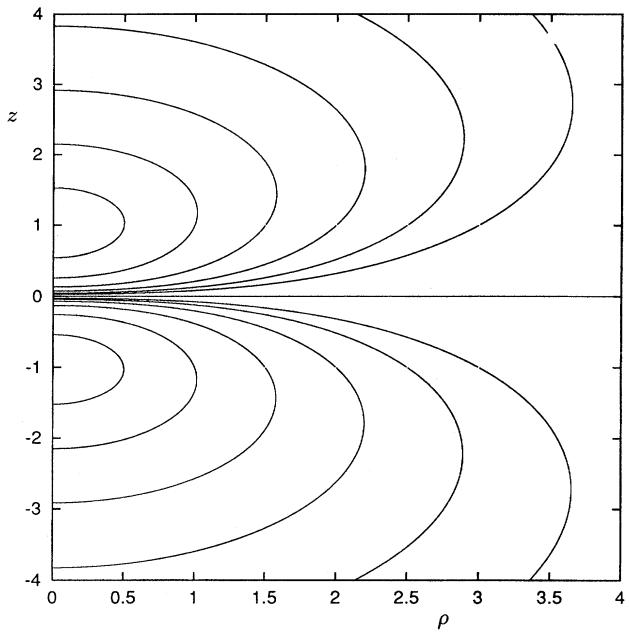

FIG. 16. Level sets of potential energy $V(\rho,z)$ for the finite dipole.

sect. A single well exists in the region labeled TC1, where $\alpha > \mu/2$; a double well exists in the region TC2, where $\alpha < \mu/2$. The small area between Σ_G^+ and the α axis is eliminated by the condition $\alpha < |E|$.

What happens when $\mu = \mu_c$? Figure 14 provides the answer. In this special case the surfaces Σ_F^1 and Σ_G^+, and the plane $\alpha = \mu/2$ all meet at the single point P. Hence the region TC2 shrinks to zero and only a single well is possible. Finally, Fig. 15 illustrates the situation for $\mu > \mu_c$. Since Σ_F^1 now crosses Σ_G^+ to the left of $\alpha = |E|$, only single-well confinement is possible for $\mu > \mu_c$. Arbitrarily large α is again permitted, with $E_{\min}$ given by the intersection of Σ_F^1 and $\alpha = \mu/2$. This yields a quartic for $E_{\min}$. In summary, we conclude that the trapping region is simply connected, unbounded in α and bounded in E. Just as in the closely related Stark problem [24], the existence of a third invariant cannot confine orbits not already energy confined, in the absence of a saddle point.

IV. FINITE DIPOLE

The finite dipole has no astronomical analog, and an accordingly briefer history. It was first treated tangentially by Fermi and Teller [32], and later in detail by Turner and Fox [15–17], where the motivation was to estimate the minimum dipole strength required to bind an electron. Figure 16 depicts level sets for the potential energy $V = 1/r_2 - 1/r_1$.

A. Effective potential

From (2.5), the effective potential is, with $\sigma = -1$,

$$U(\rho,z) = \frac{\mu}{2\rho^2} + \frac{1}{r_2} - \frac{1}{r_1}. \tag{4.1}$$

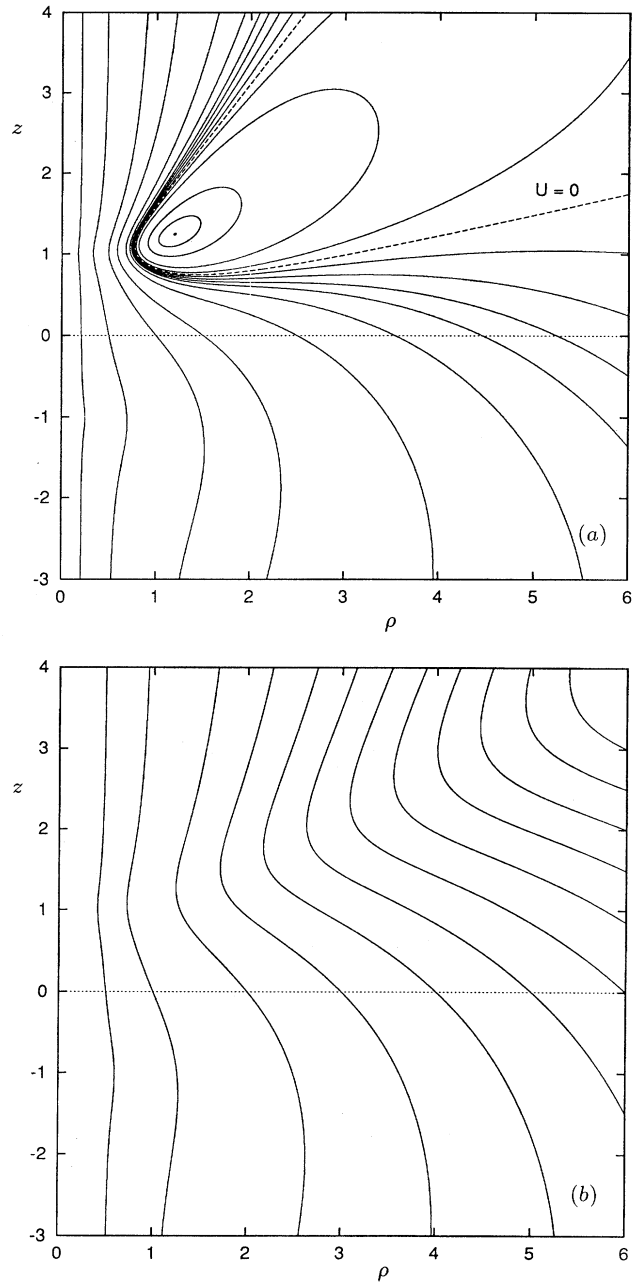

FIG. 17. Level sets of effective potential $U(\rho,z)$ for the finite dipole for (a) $\mu = 1.0$ and (b) $\mu = 2.0$. The potential well exists for all $\mu < \mu_c = 1.539$. The separatrix ($U = 0$) is indicated by the dashed curve in (a).

Figure 17 shows level sets of U for $\mu = 1.0$ and 2.0. In the first case there is a single potential well, not unlike a jelly bean, which has evidently disappeared at the larger value of μ. The critical points are given by

$$U_\rho = -\frac{\mu}{\rho^3} + \rho\left[\frac{1}{r_1^3} - \frac{1}{r_2^3}\right] = 0,$$
$$U_z = \frac{z-1}{r_1^3} - \frac{z+1}{r_2^3} = 0. \tag{4.2}$$

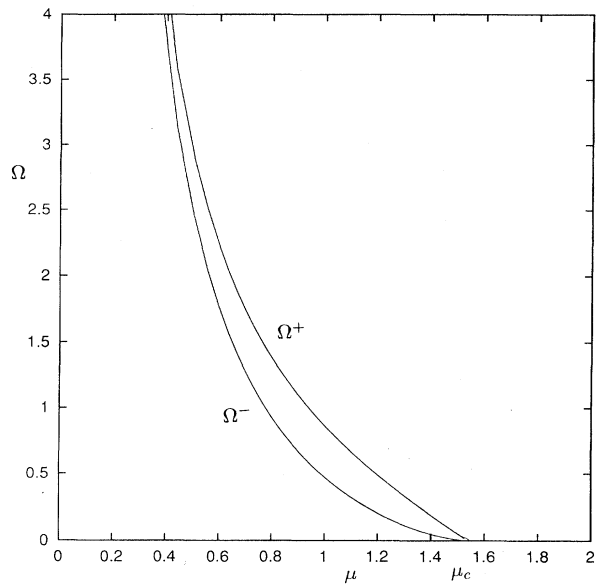

FIG. 18. Normal-mode frequencies for the finite dipole.

Equatorial equilibria are clearly impossible. As in the case of the two-center problem the second of these equations is solvable for $\rho_0(z_0)$. However, care must be taken to restrict $|z|>1$ in order to exclude extraneous solutions. The resulting locus of circular orbits is shown as the upper curve in Fig. 4, along with the corresponding locus for two centers. The first equation then gives the corresponding value of μ. What happens for large μ? Equation (3.10) allows equilibria for arbitrarily large ρ and z. However, using the asymptotic expression $\rho_0 \approx \sqrt{2} z_0$ in (4.2) shows that

$$\lim_{z\to\infty} \mu = \tfrac{8}{9}\sqrt{3} = \mu_c . \tag{4.3}$$

That is, there is no potential well for $\mu > \mu_c$. This unexpected and important result, which accounts for the disappearance of the jelly bean in Fig. 17, has apparently gone unnoticed until now. As in the case of the two center problem, the fixed point ρ_0, z_0 is born out of the source point (0,1), near which $\rho_0 \approx \mu$ and $z_0 \approx 1 + \frac{1}{4}\mu^3$. Numerical evaluation of the Hessian determinant confirms the stability of the critical point for all $\mu < \mu_c$.

Physically, condition (4.3) implies that a classical electron of arbitrary angular momentum p_ϕ can be trapped by a dipole of strength

$$p > \frac{3\sqrt{3} p_\phi^2}{4me}, \tag{4.4}$$

in agreement with Fox's result for the point dipole [16]. That is, classical bound states exist for an arbitrarily small dipole moment. Our quantitative result (4.4) sharpens the qualitative result of Turner and Fox [15]. In contrast, quantum-mechanical calculations show that a minimum dipole moment is required to bind an electron.

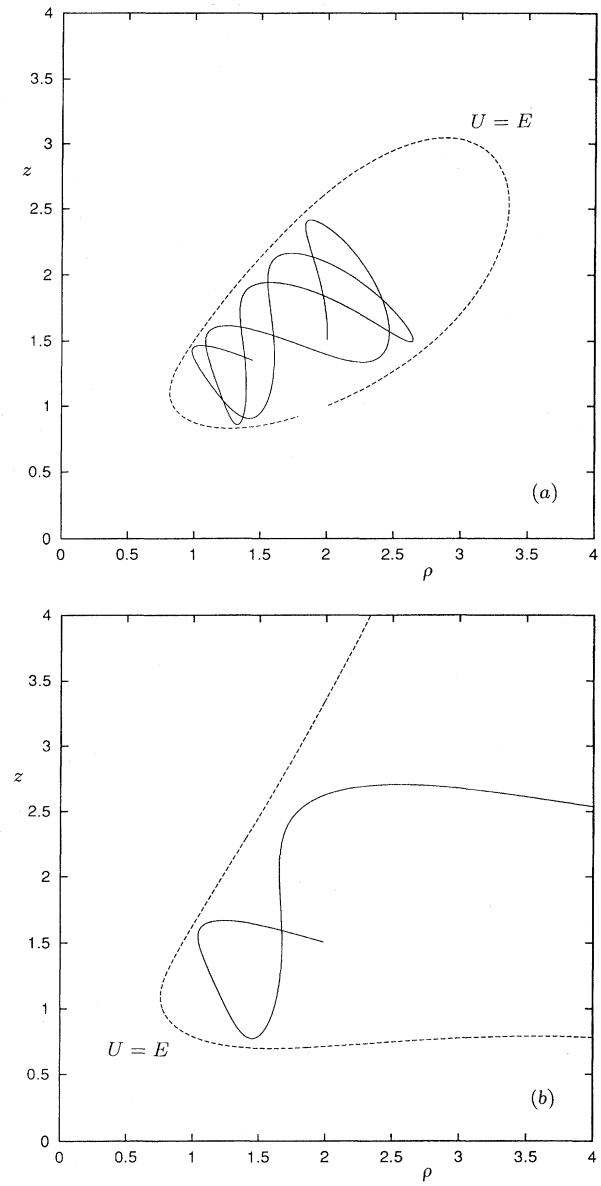

FIG. 19. Particle orbits in the finite dipole for $\mu=1$ and (a) $E=-0.0251$ (trapped) and (b) $E=0.01$ (untrapped), all in scaled atomic units.

Normal modes

The normal-mode analysis closely parallels that for the problem of two centers. The results are summarized in Fig. 18, which shows the libration frequencies $\Omega_\pm$ as a function of μ. Both are seen to decrease monotonically with increasing μ, vanishing at $\mu=\mu_c$, where the critical point runs off to infinity. As for the problem of two centers, the two modes are nondegenerate, but in this case are too close to distinguish as fast and slow modes.

B. Particle trapping

Figure 19 shows trapped and untrapped orbits in the finite dipole for $\mu=1$. In the first case ($E=-0.0251$) the orbit is

confined by energy conservation. The second plot illustrates a typical untrapped positive energy orbit ($E=0.01$). In this field, all positive energies are untrapped, while negative-energy orbits can be trapped in a potential well by energy conservation. The existence of the third invariant does not confine any particles not already trapped by energy conservation. Its sole effect would seem to be to limit the volume available to an orbit trapped in a potential well, as can be seen in Fig. 19(a). The underlying reason for the impotence of the third invariant in this case seems to be the lack of a hyperbolic critical point of U, in contrast to the Stark and two-center problems. Nevertheless, it is of interest to discover the values of all three invariants corresponding to trapped orbits. This not only furnishes independent proof of particle trapping, but, more importantly, establishes necessary information for semiclassical quantization.

As noted in Sec. II, the separated Hamiltonians for $\sigma=\pm 1$ map into one another upon interchange of ξ and η. Thus

$$\begin{aligned} &\tfrac{1}{2}(\xi^2-1)p_\xi^2+\frac{\mu}{2(\xi^2-1)}-E\xi^2=-\alpha,\\ &\tfrac{1}{2}(1-\eta^2)p_\eta^2+\frac{\mu}{2(1-\eta^2)}+E\eta^2+2\eta=+\alpha. \end{aligned} \tag{4.5}$$

Just as in the problem of two centers, the third invariant has a geometric interpretation, given implicitly by Coulson and Joseph [31]:

$$\Omega=\mathbf{L}_1\cdot\mathbf{L}_2+2(\cos\theta_1+\cos\theta_2), \tag{4.6}$$

where again $\mathbf{L}_1$ and $\mathbf{L}_2$ are the angular momenta of the test particle with respect to the two source masses, and θ_1 and θ_2 are the respective central polar angles. It is not difficult to show that the relation $\Omega=\alpha+|E|$ also holds for trapped orbits in the finite dipole. The trapping polynomials are

$$\begin{aligned} F(\eta)&=\eta^4-A\eta^3-B\eta^2+A\eta-C\leqslant 0,\\ G(\xi)&=\xi^4-B\xi^2-C\leqslant 0, \end{aligned} \tag{4.7}$$

where A, B, and C are given by (3.25). However, since ξ and η are defined on different domains, the trapping conditions are somewhat different.

Proposition II. An orbit with parameters (E,μ,α) is trapped iff *both* (i) $F(\eta)$ is negative between two positive zeros (η_1,η_2) with $\eta_1\in[-1,1]$, and $\eta_2\geqslant 0$; and (ii) $G(\xi)$ is negative between two zeros (ξ_1,ξ_2) with $\xi_1\geqslant 0$ and $\xi_2\geqslant 1$.

In contrast to the two-center problem, particle trapping in the finite dipole has not been extensively studied. While Fox [16] has proven the important fact that trapped orbits exist in the finite dipole, he did not classify orbits nor derive conditions for their existence. Nor did he mention the flight of the potential well as $\mu\to\mu_c$. We now carry out this analysis, emphasizing the three-dimensional case and only briefly treating the nonphysical meridional classes.

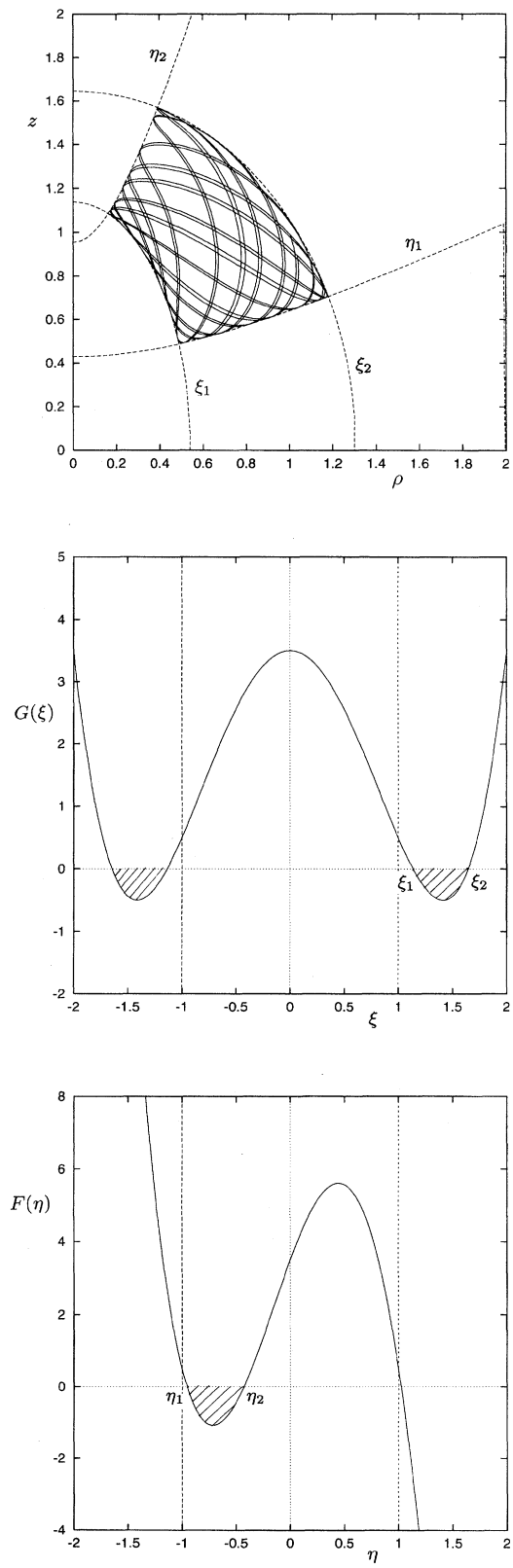

FIG. 20. Three-dimensional trapped orbit and corresponding trapping polynomials for the finite dipole.

Meridional orbits

When $\mu=0$ there are only two classes of trapped meridional orbits: pendular orbits confined to the z axis ($\Omega=0,2$), and a class of satellite electron orbits localized about the positive charge for $-2<\Omega<0$, $\alpha<0$. There are no counterparts to the planetary and lemniscate orbits encountered in the two-center problem. Of course, the region between the two source charges does not exist in real atoms and molecules, where the dipole term in V is only the first term in a multipole expansion. Only a class of pendular orbits confined to the portion of the z axis above the positive charge can be physically realized. Nevertheless, these families of orbits are important in understanding the three-dimensional orbits which unfold from them for $\mu>0$.

Three-dimensional orbits

When $\mu>0$ there is only one class of trapped orbits, occupying a singly connected toroidal region around the positive charge, as already seen in Fig. 19. Even though ξ and η are reversed, the basic conditions on F and G are identical to those for two centers, namely $F(0)=G(0)=(\mu-2\alpha)/2|E|$, $F(\pm1)=G(\pm1)=\mu/2|E|>0$, $F'(\pm1)=\pm2/|E|(\Omega\mp2)$, and $G'(\pm1)=\pm2\Omega/|E|$. First consider the form of $G(\xi)$. In order to have $G(\xi)<0$ between $\xi_1,\xi_2>1$, $G'(1)$ must be negative and $G(0)$ positive, as depicted in Fig. 20. This requires that $\Omega<0$ and therefore $\alpha<-|E|$. Further, $\Delta(G)$ must be positive, which implies $\Omega^2>2\mu|E|$. Now consider the form of $F(\eta)$. We know that $F(0)>0$ and $F(\pm1)>0$, with $F'<0$. This means that $F(\eta)$ must have a minimum greater than 1 and a minimum and maximum in $(-1,1)$, as depicted in Fig. 20(c). The trapping region in the space of the three invariants $|E|$, α, and μ is defined by the same surfaces Σ_F and Σ_G as in the case of two centers, defined by the vanishing of the respective discriminants. However, for the finite dipole the constraint $\alpha<-|E|$ eliminates the upper branch Σ_F^1. The resulting trapping region is bounded by Σ_F^2, Σ_G^-, and the negative α axis. For $\mu=\mu_c$, Σ_F^2 passes through the origin (Fig. 14) and the trapping region vanishes.[1] For $\mu>\mu_c$, Σ_F^2 intersects the *positive* α axis and there are no trapped orbits. Figure 21 presents a perspective view of the simply connected three-dimensional trapping volume, bounded by the surfaces Σ_F^2 and Σ_G^-, the α-μ plane, and the α-$|E|$ plane. It is seen to resemble a triangular pyramid, terminating at the point $(0,0,\mu_c)$, where the three surfaces intersect. When $\mu\to0$, Σ_G^- becomes the line $\alpha=-|E|$, the two sheets Σ_F^2 and Σ_F^3 merging into the line $\alpha=-2-|E|(\Omega=-2)$, as depicted in Fig. 21. In this limit the edge formed by the transverse intersection of Σ_F^2 and Σ_G^- is gradually washed out as both sheets spread out and become tangent to the α-$|E|$ plane. The trapping region is quite similar to that for the Stark problem [33].

V. POINT DIPOLE

The ideal electric dipole is an important example of an elementary integrable system and is discussed in many textbooks on mechanics [19] and electromagnetism [18]. As a limiting case of the finite dipole, it is, by virtue of its simplicity, often used as a model for both classical and quantal descriptions of experimental phenomena. Fox [16] classified the possible motions and proved the existence of (circular) bound states, but did not consider their stability. Chandrasekaran and Wilkerson [34] analyzed the meriodional and three-dimensional motion in detail, expressing the orbit in terms of elliptic functions. Several studies have addressed the important problem of determining the minimum dipole moment required to bind an electron. The results show that whereas H_2O will trap an electron H_2S cannot. As in the case of the finite dipole our primary aim is to derive explicit conditions for particle trapping, using both the effective potential and the three invariants.

Consider an electric dipole located at the origin and oriented along the z axis, i.e., $\mathbf{p}=p\hat{\mathbf{z}}$. The Hamiltonian for a positive test charge moving in this field is, in atomic units and spherical polar coordinates,

$$H=\frac{1}{2}\left(p_r^2+\frac{p_\theta^2}{r^2}+\frac{p_\phi^2}{r^2\sin^2\theta}\right)+\frac{p\cos\theta}{r^2}, \tag{5.1}$$

where $p_r=\dot{r}$, $p_\theta=r^2\dot{\theta}$, and $p_\phi=r^2\sin^2\theta\dot{\phi}$. Since ϕ is cyclic, p_ϕ is conserved and we may again define an effective potential

$$U(r,\theta)=\frac{p_\phi^2}{2r^2\sin^2\theta}+\frac{p\cos\theta}{r^2}. \tag{5.2}$$

Figure 22 depicts level sets of the dipole potential $V=p\cos\theta/r^2$. As in the case of the finite dipole, it is convenient (and desirable) to scale such that U depends on a single parameter, here $\mu=2p_\phi^2/p$:

$$U(r,\theta)=\frac{\mu}{2r^2\sin^2\theta}+\frac{2\cos\theta}{r^2}. \tag{5.3}$$

This scaling is chosen to be consistent with that for the finite dipole. Figure 23 shows level sets of U for $\mu=1.0$, 1.5396, and 2.0. Note the absence of isolated critical points and the intriguing cleft for $\mu=1.5396$, about which we shall have more to say presently. Clearly, trapped orbits must have negative total energy E and scattering orbits positive E. The separatrices are given by setting $U=E=0$, which implies that the angular function

$$g(\theta)=\frac{\mu}{2\sin^2\theta}+2\cos\theta=0, \tag{5.4}$$

which is equivalent to a cubic in $x=\cos\theta$:

$$P_0(x)=x^3-x-\frac{\mu}{4}=0. \tag{5.5}$$

As Fox has shown [16], this equation has two negative zeros $x(\mu)$ in the range $-1<x<0$ for all $\mu<\mu_c=8\sqrt{3}/9$. The dependence of the corresponding angular bounds $\theta_{a,b}$ on μ is depicted in Fig. 24. For $\mu\ll1$ the potential well occupies most of the lower quadrant. As $\mu\to\mu_c$, θ_a and θ_b merge and

[1]This limit is singular. More precisely, when $\mu=\mu_c$, $\lim_{\alpha,|E|\to0}|E|^6\Delta(F)=0$.

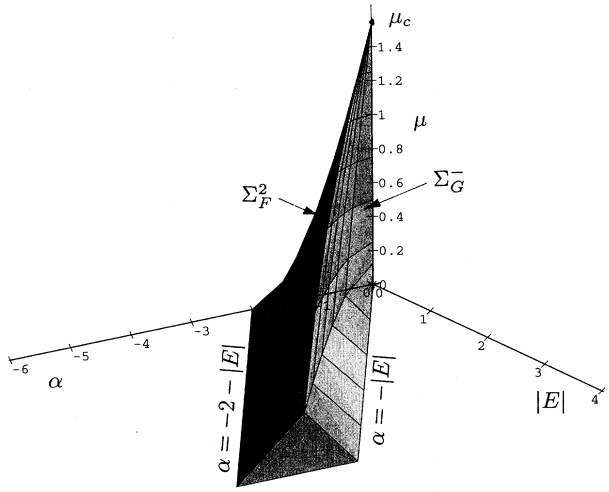

FIG. 21. Perspective view of trapping region in the space of invariants $(|E|,\alpha,\mu)$ for the finite dipole. This region is bounded by the surfaces Σ_G^-, Σ_F^2, the α-μ plane and the α-$|E|$ plane. As $\mu\to 0$ the surface is asymptotic to the α-$|E|$ plane within the diagonal region bounded by the lines $\alpha=-|E|$ and $\alpha=-2-|E|$. Here this portion of the figure has been truncated at $|E|=4.5$.

the well disappears. Just as in the case of the finite dipole there is no potential well and therefore no trapped orbits for $\mu>\mu_c$.

It is easily shown that U is a Stäckel potential [19], so that the motion is completely integrable. Thus

$$H=\tfrac{1}{2}p_r^2+\frac{1}{2r^2}\left(p_\theta^2+\frac{\mu}{\sin^2\theta}+4\cos\theta\right)=E \tag{5.6}$$

or

$$p_r^2+\frac{\alpha}{r^2}=2E, \tag{5.7}$$

where

$$\alpha=p_\theta^2+\frac{\mu}{\sin^2\theta}+4\cos\theta=L^2+4\cos\theta \tag{5.8}$$

is the third invariant, which tends smoothly to Ω [Eq. (4.5)] for the finite dipole as $a\to 0$. From (5.7) it follows that

$$r(t)=\sqrt{2Et^2+2r_0\dot{r}_0t+r_0^2}, \tag{5.9}$$

where r_0 and $\dot{r}_0$ are the initial radius and radial velocity. The θ motion follows straightforwardly from (5.8), and is reported in detail in Chandrasekaran and Wilkerson [32].

For positive E, r increases without bound, while for negative E the particle invariably plunges to the origin in a finite time $\tau=-r_0\dot{r}_0/E$. For $E=0$ *and* $\dot{r}_0=0$, $r=r_0$, i.e., the motion is confined to the surface of a sphere, which leads to the bound state discussed by Fox. Figure 25 shows typical bound and scattering orbits, along with the corresponding invariant curves.

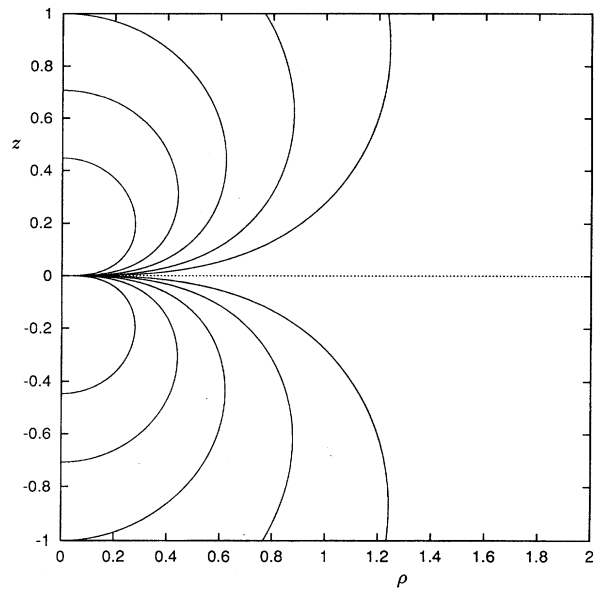

FIG. 22. Level sets of the potential energy for the point dipole.

A. Critical-point analysis

Writing

$$U(r,\theta)=\frac{1}{r^2}g(\theta), \tag{5.10}$$

with $g(\theta)$ given by (5.4), we seek relative equilibria (r_0,θ_0) via

$$U_r=-\frac{2}{r^3}g(\theta)=0,$$

$$U_\theta=\frac{1}{r^2}g'(\theta)=0. \tag{5.11}$$

That is, r_0 is arbitrary and θ_0 is a double zero of $g(\theta)$. (We leave it as an exercise for the reader to show that the Hessian determinant vanishes identically and therefore that the type of critical point is undetermined.) The value of θ is thus given by the simultaneous equations

$$\mu+4\sin^2\theta\cos\theta=0,$$

$$\mu\cos\theta+2\sin^4\theta=0. \tag{5.12}$$

Eliminating μ yields

$$\sin^2\theta(3\cos^2\theta-1)=0 \tag{5.13}$$

or

$$\cos\theta_0=-\sqrt{3}/3. \tag{5.14}$$

Substituting this value in (5.12) then gives

$$\mu_c=\frac{8}{9}\sqrt{3}, \tag{5.15}$$

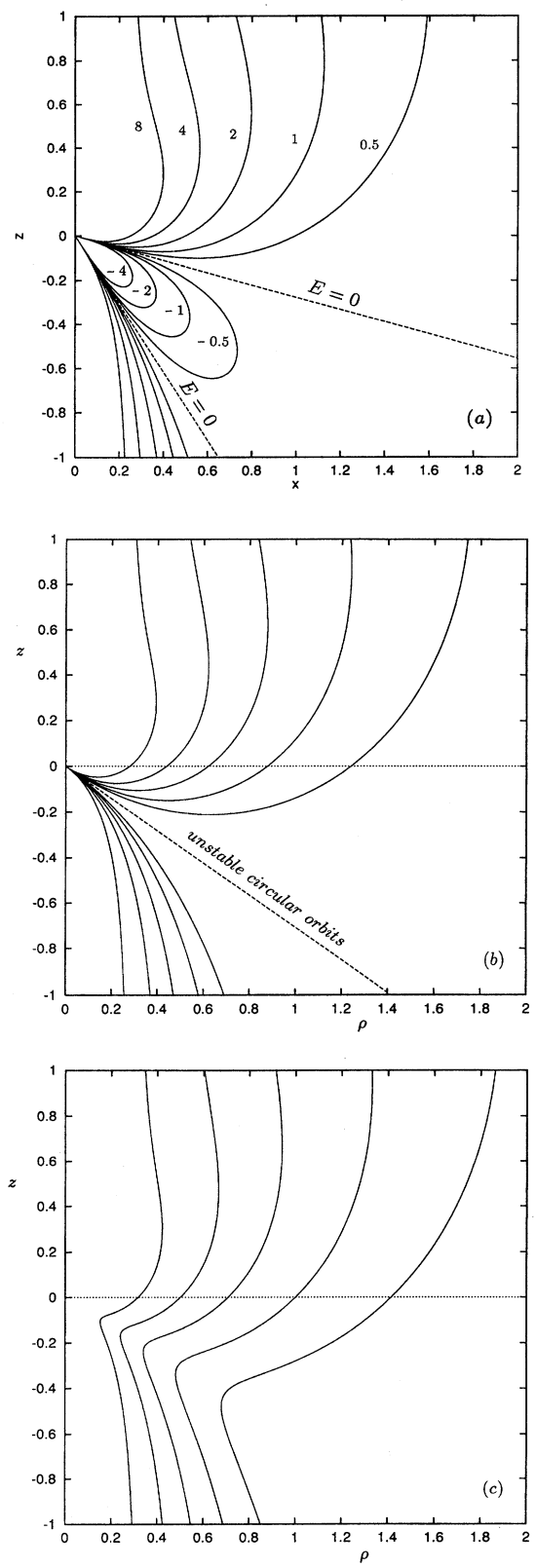

FIG. 23. Level sets of the effective potential for the point dipole with $\mu=1.0$, 1.5396, and 2.0. For $\mu=\mu_c$ a line of unstable circular orbits exists along the cleft at $\theta_0=125.26°$.

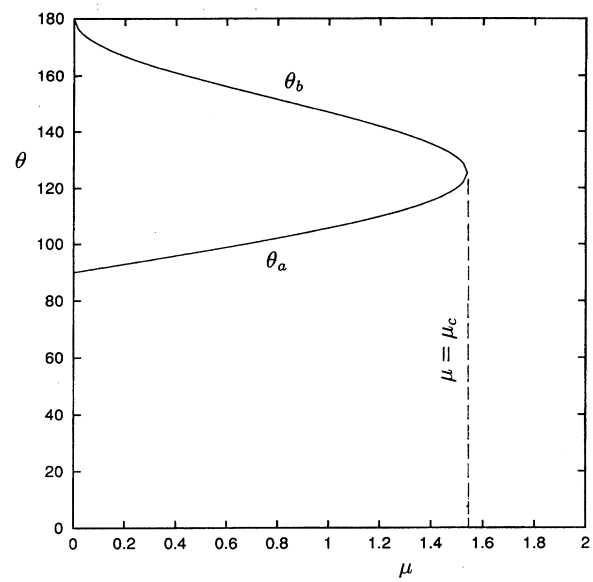

FIG. 24. Angular bounds $\theta_{a,b}$ for the potential well for the point dipole, as a function of μ. For $\mu \ll 1$ the well occupies most of the lower quadrant $\pi/2<\theta<\pi$. When $\mu \to \mu_c$ the two rays merge and the well is closed off.

at which point the two bounding rays $\theta_{a,b}$ merge, as in Fig. 24. Since $p_r=p_\theta=0$, it follows that $E=0$. Thus, for the particular energy $E=0$ and scaled angular momentum $\mu=\mu_c$, there is a line of circular orbits at an angle of $-35.26°$ with the x axis. This line is precisely the curious cleft encountered in Fig. 23(b).

B. Classification of orbits

From (5.7) and (5.8) we see that an orbit with energy E, scaled angular momentum μ, and third invariant α is constrained to move in the wedge

$$\frac{\mu}{\sin^2\theta}+4\cos\theta \leqslant \alpha, \tag{5.16}$$

$$r^2 \geqslant \frac{\alpha}{2E}. \tag{5.17}$$

Fox [16] classifies orbits in terms of the initial radial velocity $\dot{r}_0$ and position r_0. Here we adopt a Hamiltonian viewpoint and focus on the three invariants, which control the form of the effective potential U. In shifting the point of view from initial conditions to invariants, we also change the nature of the question to be answered, namely, what values of μ and α yield possible physical motions?

Radial motion

Case 1: $\alpha>0$ (potential barrier). E must be positive (scattering orbits) with r bounded from below by

$$r_{\min}=\left(\frac{\alpha}{2E}\right)^{1/2}. \tag{5.18a}$$

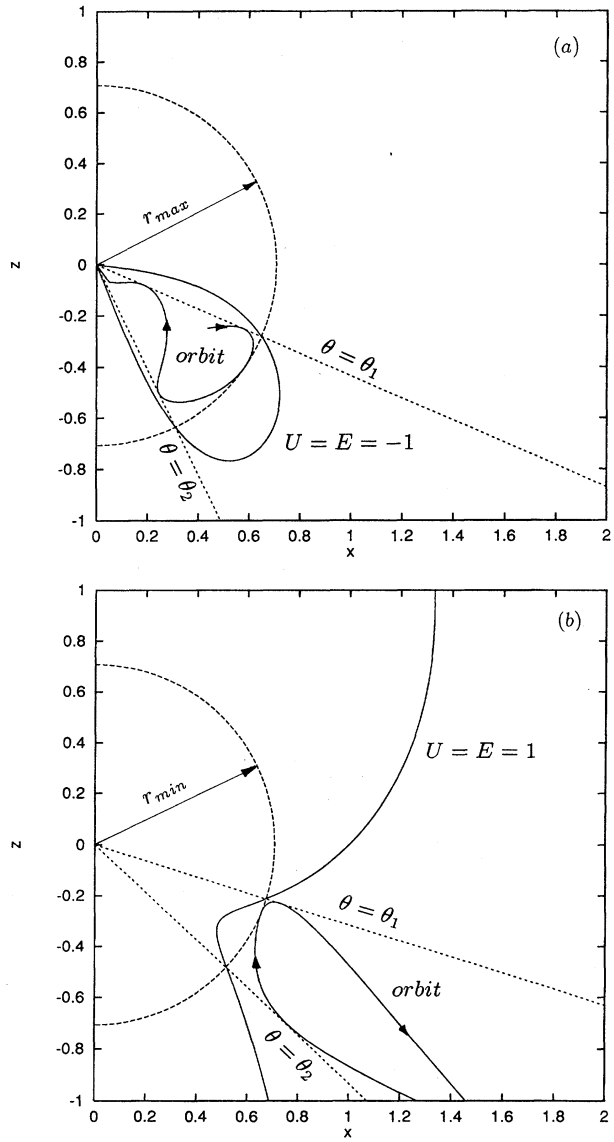

FIG. 25. Invariant curves and associated orbits for the point dipole, for (a) a trapped orbit with $\mu=0.5$ and $\alpha=E=-1$, and (b) a scattering orbit with $\mu=2$ and $\alpha=E=1$. In each case the radial and angular bounds intersect at points lying on the corresponding equipotential.

Case 2: $\alpha<0$ (potential well). If $E>0$, then p_r can never vanish; all orbits are unbounded. If $E<0$, then r is bounded from above by

$$r_{\max}=\left(\frac{\alpha}{2E}\right)^{1/2}. \tag{5.18b}$$

Case 3: $\alpha=0$ (no well). All orbits have positive energy and move with constant radial velocity outward to infinity or inward to the origin, depending on the direction of the initial velocity.

Radial bounds calculated from Eqs. (5.18) are shown for typical trapped and scattering orbits in Fig. 25.

Angular motion

Inequality (5.16) limits the angular motion and is conveniently written

$$P(x)=4x^3-\alpha x^2-4x+\alpha-\mu\geqslant 0 \tag{5.19}$$

with $x=\cos\theta$. We seek conditions on α and μ such that $P(x)$ is positive in some interval $(x_1,x_2)\in[-1,1]$. Since $P(x)$ is cubic, complex zeros are thereby excluded, requiring that the discriminant $\Delta(P)\geqslant 0$.

By definition,

$$\Delta(P)=\prod_{i<j}(x_i-x_j)^2. \tag{5.20}$$

It is a straightforward exercise in the classical theory of equations to show that [28]

$$27\,648\Delta(P)=(\alpha^2+48)^3-(\alpha^3-144\alpha+216\mu)^2. \tag{5.21}$$

Thus, for chosen α, setting $\Delta=0$ gives the critical value of μ:

$$\mu^*=\frac{144\alpha-\alpha^3+(\alpha^2+48)^{3/2}}{216}. \tag{5.22}$$

The corresponding double zero of $P(x)$ is then

$$x^*=\frac{\alpha-\sqrt{\alpha^2+48}}{12}. \tag{5.23}$$

When $\mu>\mu^*$, Δ is negative, and there are no zeros in $[-1,1]$ and therefore no physical solution. When $\alpha=0$, $P(x)$ reduces to $P_0(x)$, which defines the separatrix rays. The angular bounds $\theta_{1,2}$ calculated from $P(x)$ are shown for a typical trapped and a scattering orbit in Fig. 25. Note that the radial and angular bounds intersect at points lying on the corresponding equipotential. These invariant curves correspond to the curves of constant ξ and η for the finite dipole, as plotted in Fig. 20.

Case 1: $\alpha>0$: $P'(+1)=2(4-\alpha)>0$ for $\alpha<4$ and $P'(-1)=2(4+\alpha)>0$ for all $\alpha>0$. Figure 26 shows $P(x)$ for $\alpha=1$ and $\mu=0.5$. Since it is always the case that $P(1)=P(-1)=-\mu$, the positivity of Δ guarantees two real roots in $[-1,1]$, even for $\alpha>4$.

Case 2: $\alpha<0$: $P'(+1)>0$ for all $\alpha<0$ while $P'(-1)>0$ for all $\alpha>-4$. Thus, provided that $\Delta>0$, we conclude that $\exists(x_1,x_2)\in[-1,1]$ for all $\alpha>-4$. Furthermore, since $P'(0)=-4$, x_1 cannot be positive. Since $P(0)=\alpha-\mu$, it follows that $x_2>0$ if $\alpha>\mu$, while if $\alpha<0$ both x_1 and x_2 are negative. Since $P'(-1)<0$ for $\alpha<-4$ there are no zeros of $P(x)$ in $[-1,1]$ in this case. For example, for $\alpha=1$, $\mu^*=2.25$ and $x^*=0.5$; for $\alpha=-1$, $\mu^*=0.925\,93$ and $x^*=-0.666\,67$.

Case 3: $\alpha=0$: Here (5.19) reduces to $P_0(x)=4x^3-4x-\mu$, which has a double zero at $x^*=-\sqrt{3}/3$ when $\mu^*=\mu_c=8\sqrt{3}/9$.

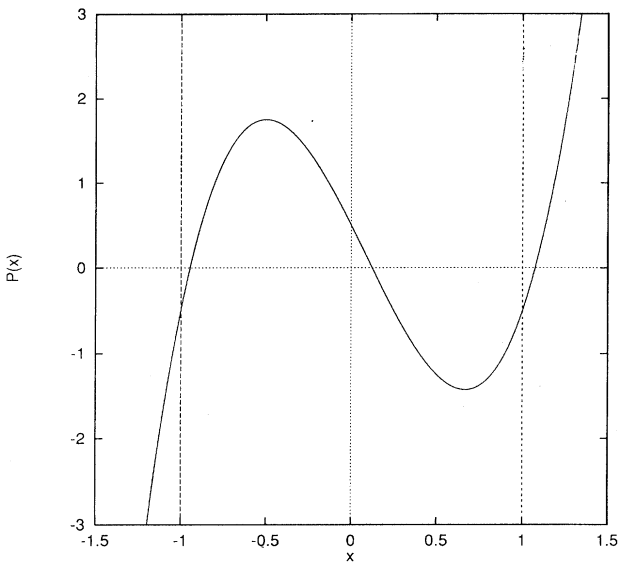

FIG. 26. Trapping polynomial $P(x)$ for the point dipole for $\alpha=1$ and $\mu=0.5$. Since $P(x)$ is positive between $x_1=-0.301$ and $x_2=-0.682$, all orbits with this α and μ are bounded by the rays $\theta_1=107.5°$ and $\theta_2=133°$.

Remark: It is not always necessary to solve (5.22) for μ^*. Since $P(0)=\alpha-\mu$, it is sufficient that $\alpha>\mu$. If $\alpha<\mu$, then μ^* must be evaluated.

VI. DISCUSSION

We have studied in some detail three closely related integrable systems: the problem of two centers, the finite dipole, and the point dipole. Each is of considerable interest in itself, both because of its myriad physical applications, but also by virtue of the unusual mathematical property of complete integrability. In each case we have emphasized the qualitative features of the effective potential, long overlooked in favor of the separated equations [in elliptic coordinates for the cases of two centers and the finite dipole (TC-FD)]. Thus a critical point analysis of U reveals interesting bifurcations in the TC problem, with important differences between the symmetric and asymmetric varieties. The surprising disappearance of the potential well at a critical value of μ in the finite dipole is apparently completely new. Neither transition is obvious in the separated equations. These methods are especially important in analyzing nonintegrable perturbations of the TC-FD problems, such as the magnetic TC problem, which is axisymmetric and therefore possesses an effective potential. As in the chaotic Stark-Zeeman system, the unperturbed integrable system provides a springboard for analyzing the complete perturbed problem.

We have also carried out a complete algebraic solution of the problem of characterizing three-dimensional trapped orbits in the symmetric TC and FD problems. These results directly impact the semiclassical quantization of the corresponding atomic systems such as H_2^+ and HeH^{2+}, and dipolar molecules such as H_2O and H_2S. The corresponding solution for unequal masses introduces a fourth independent parameter, and requires use of Sturm's theorem to derive a complete set of trapping conditions. This calculation will be reported elsewhere [25].

It is interesting and instructive to examine the several connections between these physically different but mathematically very similar systems. Thus the potential wells in TC and FD both undergo dramatic metamorphoses when a control parameter crosses the same critical value. Owing to a previously unrecognized symmetry in the separated Hamiltonians, the trapping polynomials F and G are identical in the two systems, albeit defined on different domains. The geometric form of the third invariant is very similar for the two-center problem and the finite dipole, the latter tending smoothly to the familiar invariant for the point dipole as the charge separation goes to zero.

This paper is one in a series devoted to integrable systems in atomic physics. Previous articles dealt with integrable cases of two-ion motion in a Paul trap [26,27]. This system undergoes a pitchfork bifurcation, forming a double well strikingly similar to that seen in the symmetric two-center problem. More recently we examined the interesting connections between saddle-point ionization and the third invariant for the Stark problem [24]. Here the third invariant can confine particles untrapped by energy conservation, but only in the presence of a hyperbolic fixed point of the effective potential. An analogous result holds in the two-center problem, where the third invariant can trap particles locally in one half of the double well. In contrast, the finite dipole does not possess a saddle point for any choice of parameters. Hence, the third invariant cannot trap any orbits not already confined by energy conservation.

ACKNOWLEDGMENTS

We would like to thank Roger Broucke and Charles Schwieters for helpful discussions. This work was supported in part by the Computer Services Department at Utah State University, ONR through a grant to the College of William and Mary, JILA, the Institute for Physical Science and Technology (University of Maryland), and Environmental Science Communications, Inc. We are grateful to the Program in Applied Mathematics at the University of Colorado for their hospitality during the latter phases of this work, and to Steve Collins (Utah State) for assistance in producing the figures.

APPENDIX: LEMMA ON BIFURCATIONS OF AXISYMMETRIC EQUILIBRIA

Consider a general two-dimensional effective potential

$$U(\rho,z)=\frac{\mu}{2\rho^2}+V(\rho,z), \tag{A1}$$

where $V(\rho,z)$ is an arbitrary smooth axisymmetric potential, which may or may not be harmonic. In addition to the two-center problem and the finite dipole, this includes the Stark problem [24], the magnetic two-center problem [22], with $\mathbf{B}=B\hat{\mathbf{z}}$, the $\mathbf{E}\|\mathbf{B}$ problem [24], and two-ion motion in the Paul trap and Penning trap [26,27].

The equilibria are given by

$$U_\rho = -\frac{\mu}{\rho^3} + V_\rho = 0, \tag{A2}$$

$$U_z = V_z = 0. \tag{A3}$$

Let Γ be the locus of equilibria defined by (A3). Then we have the following lemma.

Lemma. The function $\mu(\rho,z) = \rho^3 V_\rho$ reaches an extremum at a bifurcation point in proceeding along Γ.

Proof. From (A3), $d\rho/dz = -U_{zz}/U_{\rho z}$ on Γ. Hence, explicitly,

$$\frac{1}{\rho^3}\left(\frac{d\mu}{dz}\right)_\Gamma = V_{\rho z} + \left(V_{\rho\rho} + \frac{3V_\rho}{\rho}\right)\frac{d\rho}{dz}$$

$$= U_{\rho z} + U_{\rho\rho}\left(\frac{-U_{zz}}{U_{\rho z}}\right) = \frac{U_{\rho z}^2 - U_{\rho\rho}U_{zz}}{U_{\rho z}} = 0. \tag{A4}$$

Conversely, if $\rho \neq 0$, $d\mu/dz = 0 \Rightarrow \det D^2 U = 0$.

Remark. The nature of the extremum in general depends on the detailed structure of $V(\rho,z)$. There could, for example, be more than one extremum. In the case of the problem of two centers it is easily seen that $\mu = 0$ at both endpoints of Γ^+. Since $\mu \geqslant 0$ it follows that $d\mu/dz$ attains a local maximum at z_c.

[1] C. G. J. Jacobi, in *Vorlesungen über Dynamik*, edited by A. Clebsch (Reiner, Berlin, 1866).
[2] C. L. Charlier, *Die Mechanik des Himmels*, 2nd ed. (de Gruyter, Berlin, 1927).
[3] A. Deprit (unpublished).
[4] E. T. A. Whittaker, *Analytical Dynamics*, 4th ed. (Cambridge University Press, Cambridge, 1941).
[5] E. I. Timoshkova, Cosmic Res. **5**, 134 (1966).
[6] E. P. Aksenov, Astron. Zh. **45**, 1284 (1968) [Sov. Astron. **12**, 681 (1969)].
[7] S. Chandrasekhar, Proc. R. Soc. London Ser. A **421**, 227 (1989).
[8] G. Contopoulos, Proc. R. Soc. London **431**, 183 (1990).
[9] N. Bohr, Philos. Mag. **26**, 857 (1913).
[10] W. Pauli, Ann. Phys. (Leipzig) **68**, 177 (1922).
[11] E. Fermi, Rend Lincei **1**, 77 (1925).
[12] M. Born, *Mechanics of the Atom* (Ungar, New York, 1960).
[13] E. Teller, Z. Phys. **61**, 458 (1930).
[14] M. P. Strand and W. P. Reinhardt, J. Chem. Phys. **70**, 3812 (1979).
[15] J. E. Turner and K. Fox, J. Phys. A **1**, 118 (1968).
[16] K. Fox, J. Phys. A **1**, 124 (1968).
[17] J. E. Turner, Am. J. Phys. **47**, 87 (1979).
[18] J. D. Jackson, *Classical Electrodynamics*, 2nd ed. (Wiley, New York, 1975).
[19] H. Goldstein, *Classical Mechanics*, 2nd ed. (Addison-Wesley, New York, 1983).
[20] V. I. Arnold, *Dynamics III* (Springer-Verlag, New York, 1981).
[21] I. Ben-Itzhak *et al.* Phys. Rev. A **49**, 1774 (1994).
[22] U. Kappes, P. Schmelcher, and T. Pacher, Phys. Rev. A **50**, 3775 (1994).
[23] R. L. Waterland, J. B. Delos, and M. L. Du, Phys. Rev. A **35**, 5064 (1987).
[24] J. E. Howard, Phys. Rev. A **51**, 3934 (1995).
[25] J. E. Howard and T. D. Wilkerson (unpublished).
[26] J. E. Howard and D. F. Farrelly, Phys. Lett. A **178**, 62 (1993).
[27] D. F. Farrelly and J. E. Howard, Phys. Rev. A **49**, 1494 (1994).
[28] J. E. Howard, Celest. Mech. **48**, 267 (1990).
[29] L. E. Dickson, *New First Course on the Theory of Equations* (Wiley, New York, 1939).
[30] H. A. Erickson and E. L. Hill, Phys. Rev. **756**, 29 (1949).
[31] C. A. Coulson and A. Joseph, Int. J. Quantum Chem. **1**, 337 (1967).
[32] E. Fermi and E. Teller, Phys. Rev. **72**, 406 (1947).
[33] J. E. Howard (unpublished).
[34] T. Chandrasekaran and T. D. Wilkerson, Phys. Rev. **181**, 329 (1969).

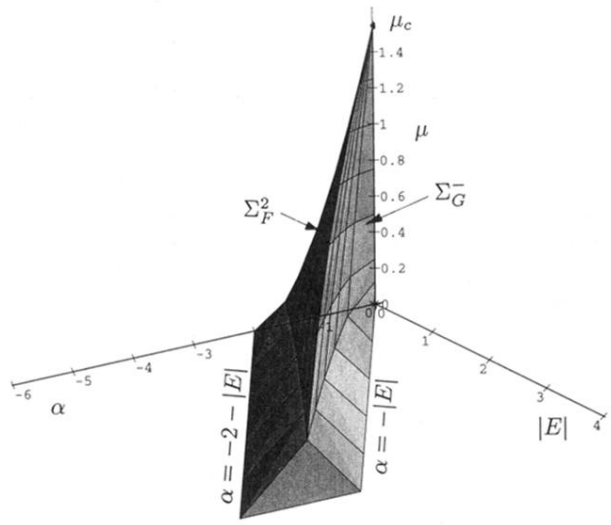

FIG. 21. Perspective view of trapping region in the space of invariants $(|E|, \alpha, \mu)$ for the finite dipole. This region is bounded by the surfaces Σ_G^-, Σ_F^2, the α-μ plane and the α-$|E|$ plane. As $\mu \to 0$ the surface is asymptotic to the α-$|E|$ plane within the diagonal region bounded by the lines $\alpha = -|E|$ and $\alpha = -2 - |E|$. Here this portion of the figure has been truncated at $|E| = 4.5$.